Peer reviewed version

Link to published version (if available):

Link to publication record in Explore Bristol Research
PDF-document

University of Bristol - Explore Bristol Research
General rights

1 **Dynamic responses of the adrenal steroidogenic**

2 **regulatory network**

3

4 Francesca Spiga[1,†,*], Eder Zavala[2,3,4,†], Jamie J Walker [1,3,4,5,†], Zidong Zhao[1], John R

5 Terry[2,3,4], Stafford L Lightman[1,4]

6

7 [1] Henry Wellcome Laboratories for Integrative Neuroscience and Endocrinology,

8 University of Bristol, Whitson St. BS1 3NY, Bristol, United Kingdom

9 [2] Living Systems Institute, University of Exeter, Stocker Rd. EX4 4QD, Exeter, United

10 Kingdom

11 [3] Wellcome Trust Centre for Biomedical Modelling and Analysis, University of Exeter,

12 Stocker Rd. EX4 4QD, Exeter, United Kingdom

13 [4] EPSRC Centre for Predictive Modelling in Healthcare, University of Exeter, Stocker

14 Rd. EX4 4QD, Exeter, United Kingdom

15 [5] College of Engineering, Mathematics and Physical Sciences, University of Exeter,

16 North Park Rd. EX4 4QF, Exeter, United Kingdom

17

18 † Denotes equal contribution

19 * Correspondence and requests for materials

20

21 Classification: BIOLOGICAL SCIENCES, Systems Biology.

22

23 Short title: Dynamics of the steroidogenic regulatory network

24

25 Keywords: glucocorticoids, adrenal gland, stress response, mathematical model,

26 steroidogenesis.

27

28 **Abstract**

29

30 The hypothalamic-pituitary-adrenal axis is a dynamic system regulating

31 glucocorticoid hormone synthesis in the adrenal glands. Many key factors within the

32 adrenal steroidogenic pathway have been identified and studied, but little is known

33 about how these factors function collectively as a dynamic network of interacting

34 components. To investigate this, we developed a mathematical model of the adrenal

35 steroidogenic regulatory network that accounts for key regulatory processes

36 occurring at different time scales. We used our model to predict the time evolution of

37 steroidogenesis in response to physiological ACTH perturbations, ranging from basal

38 pulses to larger stress-like stimulations (e.g. inflammatory stress). Testing these

39 predictions experimentally in the rat, our results show that the steroidogenic

40 regulatory network architecture is sufficient to respond to both small and large ACTH

41 perturbations, but that coupling this regulatory network with the immune pathway is

42 necessary to explain the dissociated dynamics between ACTH and glucocorticoids

43 observed under conditions of inflammatory stress.

44

45

46

47

48

49

50

51

52

53

54

Significance

Our ability to respond to stress depends on a remarkably dynamic process of hormone secretion. The rapid release of glucocorticoid hormones from the adrenal glands is critical to mount such an efficient response to stress, particularly during inflammation. Though many key factors involved in this process have been studied, the way in which these factors interact dynamically with one another to regulate glucocorticoid secretion has not been investigated. Here, we develop a mathematical model of the regulatory network controlling glucocorticoid synthesis and, by combining this with *in vivo* experiments, show how this network governs changes in adrenal responsiveness in basal unstressed physiological conditions and under exposure to inflammatory stress.

\body

Introduction

The hypothalamic-pituitary-adrenal (HPA) axis is a stress-responsive neuroendocrine system that controls circulating levels of the vital glucocorticoid (CORT) hormones corticosterone (in rodents) and cortisol (in humans). These are steroids synthesised by the adrenal gland in response to stimulation by adrenocorticotropic hormone (ACTH), which is secreted by the anterior pituitary in response to corticotrophin-releasing hormone (CRH) and arginine vasopressin released from the hypothalamic paraventricular neurons (PVN). These neurons receive circadian inputs from the suprachiasmatic nucleus (SCN), and are activated in response to stress. Via the bloodstream, CORT accesses target tissues where it mediates metabolic, cognitive, and immune responses. CORT also regulates its own production through negative feedback inhibition of ACTH and CRH secretion from the pituitary and the PVN, respectively. In order to mount an effective response to stress, CORT must be secreted rapidly by the adrenal glands. However, because of its lipophilic nature,

83   CORT cannot be pre-stored into vesicles, and must therefore be rapidly synthesised

84   *de novo* in response to ACTH stimulation.

85

86   In basal, unstressed conditions, ACTH and CORT exhibit ultradian oscillations.

87   Although there is some evidence for pulsatility of CRH (1, 2), our recent work

88   suggests that ACTH and CORT pulsatility is predominantly generated by a sub-

89   hypothalamic oscillator within the pituitary-adrenal system (3, 4). The amplitude of

90   these pulses varies in a circadian manner, with larger pulses occurring at the start of

91   the active phase (morning in humans; evening in rodents). In normal physiological

92   conditions, CORT secretion is tightly correlated with ACTH (5). However, there are a

93   number of conditions where a dynamic dissociation between these hormones occurs

94   (reviewed in (6)). For example, there is evidence that pro-inflammatory cytokines

95   released during inflammation can potentiate adrenal responsiveness to ACTH, and

96   can activate the adrenal steroidogenic pathway directly (7). Recent examples of this

97   are the hormonal stress responses observed during cardiac surgery in humans and

98   in a rodent model of inflammation (8). It has been hypothesised that this dynamic

99   dissociation is due to increased adrenal sensitivity to ACTH, presumably as a result

100   of the effect of circulating pro-inflammatory cytokines. Thus, a better understanding

101   of the mechanisms that regulate steroidogenesis is necessary to explain the dynamic

102   response of CORT to both physiological and pathological ACTH perturbations.

103

104   Within cells of the adrenal cortex *zona fasciculata*, steroidogenesis is regulated by

105   several processes operating over a range of timescales: there are rapid non-genomic

106   processes, as well as slower processes that depend on gene expression. Together,

107   these form a complex pathway activated when ACTH binds the melanocortin type-2

108   receptor (MC2R), resulting in rapid phosphorylation of proteins involved in

109   cholesterol metabolism—the substrate for CORT synthesis. These include hormone-

110   sensitive lipase (HSL) and steroidogenic acute regulatory (StAR) proteins, which

111   control levels of intracellular cholesterol and its transport within the mitochondrial

112   matrix, respectively (9, 10). In addition to these rapid, non-genomic events, ACTH

113   simultaneously triggers a slower genomic response involving the expression of

114   steroidogenic genes such as *StAR*, *CYP11A*, *MC2R* and *MRAP*. These genes are

115   transcriptionally regulated by a number of nuclear receptors, whose activity and

116   expression is also under the control of ACTH. Specifically, ACTH induces the

117   "positive regulators" steroidogenic factor 1 (SF-1) (11) and Nur77 (NR4A1) (12), and

118   inhibits the "negative regulator" DAX-1 (dosage sensitive sex-reversal (DSS), adrenal

119   hypoplasia congenita (AHC) locus on the X-chromosome) (13). These interacting

120   cascades of genomic and non-genomic events work in combination to activate and

121   maintain optimal levels of steroidogenic proteins, ultimately leading to mitochondrial

122   import of cholesterol and CORT synthesis. In addition, our recent mathematical

123   modelling of the CORT response to ACTH suggests that a rapid, intra-adrenal CORT

124   negative feedback loop constitutes an additional control mechanism of

125   steroidogenesis (14-17). The biological processes underlying this self-inhibition are

126   not known, but the glucocorticoid receptor (GR) is expressed in the adrenal cortex

127   (15, 18). Furthermore, the synthetic glucocorticoid dexamethasone—a specific GR

128   agonist—has been shown to inhibit ACTH-induced corticosterone secretion from rat

129   adrenocortical cells (19), as well as the transcription of steroidogenic genes through

130   a mechanism that involves GR- and SF-1-mediated induction of DAX-1 expression

131   (20).

132

133   Though many of the components involved in the steroidogenic pathway have been

134   identified, it remains unclear how their mutual interaction regulates CORT dynamics.

135   In this study, we considered the core components of the steroidogenic regulatory

136   network (SRN) and investigated how the cross-talk among these components

137   underlies ACTH-responsive CORT dynamics. To understand the time evolution of

138   steroidogenesis following ACTH stimulation, we developed a mathematical model of

139   the SRN based on the complex molecular interactions within the SRN, including the

140   intra-adrenal GR-CORT connection that feeds back on the genomic pathway. We

141   used this model to characterise dynamic responses to a variety of perturbations, and

142   to make predictions that we then tested experimentally. Our results show that it is the

143   complex interactions between components of the SRN that governs dynamic

144   steroidogenic responses in adrenocortical cells. Importantly, the SRN architecture

145   enables cells to respond to both small and large ACTH perturbations, but is not

146   sufficient to explain the dynamic response to inflammatory stress; in this case, we

147   found that the CORT response can only be explained by coupling the SRN with the

148   immune pathway. This work provides a theoretical framework to study adrenal CORT

149   responses to a range of physiological and pathological perturbations, building upon

150   our previous work on the role of glucocorticoid-mediated negative feedback loops

151   regulating the ultradian dynamics of the HPA axis (3, 4).

152

153   **Results**

154

155   **A short pulse of ACTH dynamically activates the SRN and CORT biosynthesis**

156   To explore systematically how dynamic responses result from complex interactions

157   within the SRN, we developed a mathematical model of the regulatory network. To

158   aid analysis, we restrained the complexity of the model by stripping off non-essential

159   regulatory components from the network architecture. This was performed by

160   including only those nodes within the SRN that have been shown to be involved in

161   CORT-mediated feedback loops and participate in cross-talk with StAR (Fig. 1; see

162   SI Appendix, Fig. S1 for the full SRN) (20-25). Specifically, the model consists of a

163   set of delay differential equations (DDEs) that describe the dynamics of intra-adrenal

164   levels of CORT (A-CORT) and phosphorylation of GR (pGR; a marker of GR

165   activation), and the expression of DAX-1, SF-1 and StAR following "virtual" (*in silico*)

166   stimulation by ACTH (SI Appendix, Fig. S2 and SI Appendix, Supp. Text).

167

168   To assist the calibration of our mathematical model, we first considered the response

169   of the SRN to a single pulse of ACTH, similar to an endogenous ultradian pulse of

170   ACTH (Fig. 2a). To do this, we performed an *in vivo* experiment in the rat to

171   characterise the dynamic response of the adrenal SRN to an i.v. injection of ACTH.

172   We measured both those factors in the core SRN (Fig. 1), as well as some additional

173   factors that are also involved in steroidogenesis but were not considered in the

174   model. The i.v. ACTH injection resulted in a rapid and transient increase in plasma

175   ACTH (Fig. 2a), with a peak concentration comparable to the peak of endogenous

176   ultradian ACTH pulses (26, 27). This was accompanied by a rapid and dynamic

177   increase in CORT secretion, detectable in both adrenal tissue (A-CORT; Fig 2b) and

178   blood plasma (P-CORT; SI Appendix, Fig S3b). To assess the dynamics of GR

179   activation following the i.v. ACTH injection, we measured phosphorylation of GR

180   (pGR) at Serine 211 (28). pGR demonstrated a rapid, significant increase (Fig. 2c),

181   and its pattern of activation was similar to the observed pattern of A-CORT (Fig. 2b).

182

183   ACTH also regulates steroidogenesis over a slightly slower time frame via

184   modulation of the expression of genes involved in CORT synthesis. We therefore

185   determined the effects of the i.v. ACTH injection on the dynamic expression of key

186   steroidogenic genes in the adrenal SRN. Since many ACTH-regulated genes require

187   activation of CREB in order to be transcribed, we first assessed the dynamics of

188   CREB phosphorylation (pCREB). Consistent with previous reports (29, 30), there

189   was a rapid and transient increase in pCREB (SI Appendix, Fig. S3d). We then

190   investigated the dynamic transcription of steroidogenic genes by measuring their

191   hnRNA and mRNA levels. As expected, the dynamics of pCREB was paralleled by a

192   transient activation of StAR hnRNA, followed by a slower StAR mRNA accumulation

193   (Fig. 2f,i). In response to the i.v. ACTH injection, there was a rapid, transient

194   decrease in DAX-1 hnRNA, and a dynamic increase in SF-1 hnRNA (Fig. 2d,e). In

195   contrast, no significant changes in DAX-1, SF-1, and StARp37 protein levels were

196   detected within two hours of ACTH administration (Fig. 2j-l).

197

198   With respect to those SRN factors that were not considered in the model, we found

199   that the i.v. ACTH injection also had a rapid effect on the activity of hormone-

200   sensitive lipase (HSL), a protein that plays a key role in the CORT SRN by regulating

201   intracellular metabolism of cholesterol (SI Appendix, Fig. S3c). We assessed this by

202   measuring the phosphorylation dynamics at sites known to increase HSL activity

203   (pHSL at Serine 660 and 563) (31), and observed a dynamic activation of both

204   pHSL-(Ser660) and pHSL-(Ser563). This suggests that a rapid, transient increase in

205   intracellular free cholesterol precedes CORT synthesis, and supports previous

206   findings that this is a crucial step in the steroidogenic process. Furthermore, ACTH

207   rapidly activated hnRNA and mRNA levels of MC2R, MRAP, Nur77 and CYP11A1,

208   but had no effect on HSL hnRNA and mRNA (SI Appendix, Fig. S3e). However, no

209   significant changes in CYP11A1, StARp32, StARp30 or HSL protein levels were

210   detected within two hours of ACTH administration (SI Appendix, Fig. S3f). Taken

211   together, these results show that dynamic changes within both non-genomic and

212   genomic processes are involved in the dynamic regulation of steroidogenesis.

213

214   Next, we fitted the model to the experimental data (Fig. 2). In addition to recalibrating

215   model parameters, we further considered a potential post-transcriptional regulatory

216   mechanism; namely, ACTH dose-dependent control of DAX-1 mRNA stability. This

217   proposed mechanism accounts for DAX-1 mRNA levels observed following ACTH

218   stimuli of varying magnitude (32) (SI Appendix, Supp. Text and SI Appendix, Fig.

219   S4). The time-evolution of the SRN was generated by driving the mathematical

220   model with a virtual ACTH pulse given during the nadir of the circadian rhythm (SI

221   Appendix, Fig. S2 and SI Appendix, Supp. Text). These simulations showed that the

222   A-CORT dynamics exhibited a rising phase (<5 min), a peak ~10 min, and a falling

223 phase (>15 min) (Fig. 2b). Similarly, the pGR dynamics predicted by the model

224 displayed a rising phase (<5 min), a peak ~12 min, and a falling phase (>15 min)

225 (Fig. 2c). The model also predicted a transient induction of the SF-1 and StAR

226 genes, as judged from their rapidly-inducible primary transcripts (heteronuclear RNA,

227 hnRNA), mRNA, and protein dynamics (Fig. 2e,f,h,i,k,l). In contrast, the model

228 predicted a transient inhibition of DAX-1 hnRNA, but a transient induction of its

229 mRNA and protein levels (Fig. 2d,g,j). Taken together, these simulations closely

230 matched the *in vivo* data for A-CORT and pGR dynamics, as well as gene induction

231 (Fig. 2b-f). Whilst the changes in mRNA and protein levels measured *in vivo* were not

232 statistically significant, our model still reproduced the transient dynamics of DAX-1

233 mRNA and protein (Fig. 2g,j), and predicted a gradual increase of SF-1 and StAR

234 mRNA and protein (Fig. 2h,i,k,l) that is consistent with the transient increase of their

235 corresponding hnRNAs. Discrepancies between the model and experimental data

236 may originate from unexplored post-transcriptional or post-translational regulatory

237 mechanisms of SF-1 and StAR expression that the model does not account for.

238

239

240

241 **The SRN underlies the ACTH/CORT dynamic response to large perturbations**

242 **comparable to those observed during inflammatory stress**

243 Our data show that an ACTH stimulus comparable to an endogenous ultradian pulse

244 leads to dynamic changes within the SRN, ultimately driving the tightly-correlated

245 dynamic release of CORT. However, the adrenal gland is also subjected to more

246 forceful perturbations (e.g. those associated with severe stressors), and in some

247 cases the tight correlation between ACTH and CORT is lost. This "dissociation" has

248 been implicated in a change of the adrenal's sensitivity to ACTH (reviewed in (6)),

249 suggesting that the SRN has the ability to decode ACTH signals in a context-

250 dependent manner. Motivated by this, we used our model to investigate how the

251 SRN responds to a larger ACTH perturbation, comparable to that measured in

252 response to an inflammatory stress (8), and tested our model predictions

253 experimentally.

254

255 We have previously developed an experimental methodology to apply a large ACTH

256 stimulus to the rat adrenal glands (8). This consists of four sequential sub-cutaneous

257 (s.c.) injections of ACTH at 35 min intervals, which results in a large surge in ACTH

258 plasma concentrations comparable to that observed during inflammatory stress (Fig.

259 3a). To explore how such a substantial ACTH perturbation affects the dynamics of

260 components within the adrenal SRN, we drove our model with this same pattern of

261 ACTH stimulation and simulated the transient dynamics of CORT and pGR, as well

262 as DAX-1, SF-1, and StAR. Our model predicted a rapid, transient increase in A-

263 CORT consisting of a rising phase (<30 min), plateau (45 to 120 min), and falling

264 phase (>120 min) (Fig. 3b). As expected, the pGR dynamic profile predicted by the

265 model was consistent with that of A-CORT (Fig. 3c). In terms of gene expression, the

266 model predicted a transient inhibition of DAX-1 gene expression, as well as a

267 transient induction of SF-1 and StAR genes (Fig. 3d-i). Regarding protein levels, our

268 model produced a transient activation of SF-1 and StARp37, and a gradual decline in

269 DAX-1 (Fig. 3j-l).

270

271 To test these modelling predictions, we measured the dynamic response of the rat

272 SRN to this ACTH challenge. The increase in plasma ACTH levels was paralleled by

273 a robust increase in both A-CORT (Fig. 3b) and P-CORT (SI Appendix, Fig. S5b). As

274 observed in the i.v. ACTH pulse experiment, there was a dynamic increase in pGR

275 that was consistent with the observed pattern of A-CORT (Fig. 3c). Consistent with

276 the ACTH i.v. pulse data, there was a significant decrease in DAX-1 hnRNA and

277 mRNA (Fig. 3d,g), and a significant increase in SF-1 and StAR hnRNA and mRNA

278 (Fig. 3e,f,h,i). With regard to protein levels, the high dose of ACTH also induced a

279   significant increase in StARp30 (Fig. S5f), but not in StARp37 (Fig. 3l), StARp32 (SI

280   Appendix, Fig. S5f), or SF-1 (Fig. 3k). There was a non-significant decrease in DAX-

281   1 protein (Fig. 3j). The dynamic effects of a high dose of ACTH on A-CORT was

282   paralleled by an increase in both pHSL-(Ser660) and pHSL-(Ser563) (SI Appendix,

283   Fig. S5c). Furthermore, dynamic transcription of StAR was accompanied by dynamic

284   changes in pCREB (Fig. S5d), as well as a rapid increase in MRAP, Nur77 and

285   CYP11A1 hnRNA and mRNA. Unexpectedly, we observed a decrease in MC2R

286   hnRNA and mRNA, and small dynamic changes were also observed for HSL hnRNA

287   and mRNA (SI Appendix, Fig. S5e). In contrast, there was no effect on CYP11A1

288   and HSL protein (SI Appendix, Fig. S5f).

289

290   Overall, there was a good qualitative fit between our model predictions and our

291   experimental data for both small and large ACTH perturbations (Fig. 2 and Fig. 3,

292   respectively). Importantly, the network architecture and parameter values in our SRN

293   model were identical in both cases. This suggests that, for the majority of the

294   molecular species considered in the model, no new mechanisms controlling the SRN

295   dynamic response have to be introduced to explain the dynamic SRN responses to

296   ACTH stimuli of varying magnitude.

297

298   **Dynamics of adrenal glucocorticoid synthesis and SRN activity in response to**

299   **LPS**

300   Our mathematical model of the SRN suggests that the adrenal response to ACTH is

301   primarily dependent on the specific pattern of ACTH stimulation. However, in several

302   stress scenarios, the adrenal may not only be driven by ACTH, but may also be

303   influenced by other factors that modulate the SRN response. For instance, activation

304   of the immune system by administration of the bacterial endotoxin LPS is known to

305   induce CORT secretion through a robust activation of the HPA axis, as well as

306   through a direct effect at the level of adrenocortical steroidogenic cells (33).

11

307 Therefore, we investigated the dynamic pattern of adrenal activation in response to

308 such a stimulus. As previously shown (8), LPS administration induced an elevated

309 and prolonged ACTH response (Fig. 4a) that was followed by a long-lasting A-CORT

310 (Fig. 4b) and P-CORT (SI Appendix, Fig. S6b) response. Unexpectedly, despite the

311 high levels of A-CORT measured after the LPS injection, there was no significant

312 effect of LPS on pGR (Fig. 4c). An elevated and long-lasting effect of LPS was

313 observed on the genomic adrenal steroidogenic pathway, including StAR hnRNA and

314 mRNA (Fig. 4f,i), and a multiphasic effect on SF-1 hnRNA (Fig. 4e) with a small non-

315 significant increase in SF-1 mRNA (Fig. 4h). In contrast to the decrease in DAX-1

316 observed in the high ACTH dose experiment, we observed a biphasic dynamic effect

317 on DAX-1 hnRNA and mRNA (Fig. 4d,g). We also measured the effects of LPS on

318 protein levels and found that it increased the levels of StARp37 (Fig. 4l) and

319 StARp32 (SI Appendix, Fig. S6f), and caused a non-significant increase in StARp30

320 (SI Appendix, Fig. S6f). There was no effect of LPS on SF-1 protein (Fig. 4k), but we

321 observed a biphasic effect of LPS on DAX-1 protein (Fig. 4j) that was consistent with

322 DAX-1 hnRNA and mRNA.

323

324 In parallel to the effect on CORT, there was a robust and prolonged effect on pHSL-

325 (Ser660) and pHSL-(Ser563), as well as dynamic changes in pCREB (SI Appendix,

326 Fig. S6c,d). Consistent with the findings from the high ACTH dose experiment, LPS

327 induced dynamic changes in MRAP, Nur77 and CYP11A1 hnRNA and mRNA, and a

328 significant decrease in MC2R and HSL hnRNA and mRNA (SI Appendix, Fig. S6e).

329 Despite its effects on transcription, there was no effect of LPS on CYP11A1 and HSL

330 protein (SI Appendix, Fig. S6f).

331

332 Injection of LPS in the rat is also known to increase plasma cytokines in a time-

333 dependent manner (34). In addition, because LPS can also increase intra-adrenal

334 expression of cytokines, we investigated the dynamics of these in LPS-treated rats.

335   As expected, LPS induced a rapid and transient increase in IL-1β hnRNA and

336   mRNA, IL-6 hnRNA and mRNA, and TNF-α hnRNA and mRNA (SI Appendix, Fig.

337   S7a-c).

338

339   Whilst LPS increases both ACTH and cytokine levels, it is not clear whether these

340   cytokines modulate the SRN response to ACTH and the mechanisms through which

341   this may occur. To investigate this, we drove our model of the SRN with the ACTH

342   pattern generated by the LPS injection, and compared its output with the

343   experimental data (Fig. 4a). Our model roughly approximated the dynamics of A-

344   CORT and the DAX-1 hnRNA (Fig. 4b,d). In contrast, the expression dynamics of

345   SF-1 and StAR showed some discrepancies in their hnRNA dynamics (Fig. 4e,f),

346   where the model failed to reproduce the biphasic induction of these genes. Parallel to

347   A-CORT, the model predicted induction and sustained activation of pGR. This was in

348   stark contrast with our experimental data showing a lack of pGR activation despite

349   high A-CORT (Fig. 4c). Taken together, these results suggest that a model of the

350   SRN lacking cytokine regulation is not sufficient to explain its response to LPS.

351

352   **Dynamic effects of LPS-induced adrenal cytokine expression on the SRN**

353   The lack of GR activation in response to LPS, together with the fact that LPS has

354   been shown to repress GR function in other tissues (reviewed in (35), points to an

355   interaction between cytokines and the GR. Indeed, previous findings show that the

356   LPS-induced pro-inflammatory cytokine TNF-α inhibits GR phosphorylation in Serine

357   211 in human airway cells (36). In light of this, we extended our model to account for

358   cross-talk between components of the SRN and the immune pathway, and used it to

359   test whether these interactions could account for the observed response to LPS. To

360   do this, we constructed a map of the network architecture in order to elucidate its

361   effects upon steroidogenesis (SI Appendix, Fig. S8 and SI Appendix, Supp. Text). As

362   was the case for the full steroidogenic network, we simplified the map of interactions

13

363   between the immune pathway and the SRN (Fig. 5 and SI Appendix, Supp. Text).

364   Further, our time course data on cytokine mRNA levels measured in the adrenal

365   exhibits a timescale similar to cytokine protein dynamics in plasma following LPS

366   stimulation (34). Thus, we accounted for the effects that cytokines TNF-α, IL-1β, and

367   IL-6 have upon specific components of the SRN by using their mRNA time course

368   data. In other words, in addition to the high ACTH response elicited by LPS we used

369   the cytokines' dynamic profiles as additional, selective input to specific targets within

370   the SRN (SI Appendix, Fig. S9).

371

372   We modified the mathematical model to account for these cytokine effects (SI

373   Appendix, Supp. Text), and carried out computer simulations to explore the

374   steroidogenic response to LPS. The mathematical model not only predicted the

375   sustained induction of A-CORT (Fig. 6b), but also the inhibition of pGR that was

376   observed following LPS injection (Fib. 6c; compare with Fig. 4c). The model also

377   predicted the transient, multiphasic induction of SF-1 and StAR genes (Fig. 6e,f), as

378   well as the transient inhibition of DAX-1 gene expression (Fig. 6d), and their

379   associated mRNA and protein dynamics (Fig. 6g-l).

380

381   **Discussion**

382

383   Previous studies of adrenal steroidogenesis have focused on specific interactions

384   between genes and proteins involved in glucocorticoid synthesis. Whilst these

385   studies have provided important biological insight into the structure and regulation of

386   key steroidogenic factors, the dynamics of the interactions of these factors across

387   different time scales has not been considered. Indeed, using static data on individual

388   interactions within the steroidogenic pathway has not been sufficient to explain how

389   specific patterns of ACTH stimulation are translated by the adrenal into specific

390   patterns of CORT secretion.

391

392   To understand this, we explored how some of these factors interact with one another

393   in the context of a complex dynamic regulatory network. Because of the dynamic

394   nature of steroidogenesis, we developed a mathematical model of the SRN that

395   accounted for regulatory processes occurring at different time scales. Importantly, we

396   also considered an intra-adrenal CORT-mediated feedback loop whose effects were

397   previously described through mathematical modelling (17). We used our model to

398   predict the time evolution of steroidogenesis following a series of physiological

399   perturbations relevant to stress and inflammation. By testing these predictions

400   experimentally, we show how the SRN can respond to both small and large ACTH

401   perturbations, and how the coupling with the immune pathway may be necessary to

402   elicit an ACTH/CORT dissociated response during inflammation.

403

404   Mathematical models of CORT dynamics have been developed to study the origin of

405   ultradian oscillations within the HPA axis (4, 17) and the inflammatory response at

406   the adrenal level (37). However, these models do not consider the dynamic

407   molecular interactions within adrenocortical cells that occur during steroidogenesis.

408   In this study, we used a mathematical modelling approach that focuses on the

409   adrenal cell's network architecture, the interplay between fast and slow processes,

410   and post-transcriptional and post-translational control of steroidogenic genes.

411   Predictions from this model can only be of a qualitative nature, which reflects our

412   limited knowledge on the regulatory processes that we modelled phenomenologically

413   (e.g. using Michaelis-Menten and Hill type functions) and the uncertainties

414   associated with some parameter values. Another limitation relates to the fact that our

415   model did not consider all the components within the full SRN. This reflects the need

416   to simplify our computational analysis by reducing the network architecture to its core

417   components. Nonetheless, our results show that the SRN operates with the same

418   core components, network architecture, and parameter values to respond to both

419 small and large ACTH perturbations; in other words, no new mechanisms need to be

420 introduced to explain the adrenal's response to a range of ACTH stimuli.

421

422 We observed that rapid and transient CORT responses to ACTH stimulation are

423 accompanied by dynamic changes in several components within the adrenal SRN.

424 Previously, we have shown that ultradian secretion of corticosterone in the rat is

425 paralleled by pulsatile transcription of steroidogenic genes including StAR, CYP11A,

426 and MRAP, and pulsatile phosphorylation of CREB (29, 30, 38) suggesting that

427 dynamic activation of the adrenal steroidogenic pathway is important for maintaining

428 ultradian glucocorticoid secretion. In this study, we aimed to further elucidate how

429 ACTH regulates adrenocortical dynamics in response to a pulse of ACTH. To our

430 knowledge, we provide the first evidence of ultradian responsiveness at the level of

431 non-genomic mechanisms within the adrenal steroidogenic pathway (i.e.

432 phosphorylation of HSL) and within the transcriptional regulation of steroidogenic

433 gene regulators (i.e. transcription of SF-1, Nur77 and DAX-1). These findings

434 suggest that ultradian secretion of ACTH is important not only for a rapid "acute"

435 adrenal response, but also for long-term maintenance of the steroidogenic pathway

436 in basal conditions. Overall, our data suggest that dynamic events occurring within

437 the adrenal SRN are important in maintaining ultradian secretion of glucocorticoids in

438 a normal, healthy state.

439

440 While there was a good fit between the model and the hormone, hnRNA and pGR

441 data, some discrepancies were observed for mRNA and protein. The levels of mRNA

442 and protein are typically thought to depend on the transcription of the gene, but

443 additional regulatory factors such as RNA binding proteins and micro RNAs can

444 affect the stability of transcripts. Because a role for ACTH-dependent regulation of

445 mRNA stability in the adrenal cortex has been proposed (reviewed in Desroches-

16

446   ==Castan et al. 2017), we hypothesise that mechanisms such as these could explain==

447   ==the discrepancies we have observed.==

448

449   Recent data from our group suggests that, in addition to the well-known CORT-

450   mediated negative feedback at the pituitary and brain regulating HPA axis activity, an

451   intra-adrenal negative feedback involving activation of the GR can rapidly inhibit

452   ACTH-induced glucocorticoid synthesis (17). Consistent with this, there is evidence

453   that glucocorticoids can inhibit the transcription of steroidogenic genes through a

454   mechanism that involves the synergistic association of SF-1 and GR to modulate

455   DAX-1 expression (20). The present study provides further evidence to support this

456   hypothesis by showing that a rapid, transient activation of adrenal GR tightly follows

457   the dynamics of intra-adrenal corticosterone. To our knowledge, this is the first

458   proposal of a model accounting for intra-adrenal feedback regulation of

459   steroidogenesis.

460

461   Further implications of an intra-adrenal CORT negative feedback loop relate to the

462   role that the DAX-1, SF-1, and StAR genes play in controlling CORT synthesis. For

463   instance, though DAX-1 expression is critical for normal HPA organ development

464   (39-41), its role in regulating steroidogenesis in the adult is still unclear. SF-1 and GR

465   have been shown to synergistically modulate DAX-1 expression (20), which in turn

466   inhibits SF-1-mediated induction of StAR (42). ACTH is known to disrupt this SF-

467   1/GR synergistic effect on DAX-1 (20), and GR is activated by intra-adrenal CORT.

468   This suggests that DAX-1 may be acting as an organising "hub" by simultaneously

469   integrating and decoding hormone signals from both the pituitary and the adrenal to

470   control steroidogenesis. If this is the case, it is possible that changes in the way this

471   "hub" functions could lead to alterations in the way the adrenal SRN responds to

472   ACTH perturbations.

473

474 We also studied the steroidogenic response to an LPS injection. In this case, not only

475 the SRN but also the immune pathway was activated, as shown by the induction of

476 cytokines TNF-α, IL-6, and IL-1β. The cross-talk between the steroidogenic and

477 immune pathways has been modelled previously, though only at the system level

478 (37). The mathematical model we present here is the first to incorporate a detailed

479 description of the SRN and its interactions with the immune pathway. Notably, our

480 model reproduced the LPS response until we explicitly accounted for the effects that

481 cytokines have upon specific components within the SRN. This suggests that

482 cytokines interact with ACTH to mediate the inflammatory response at the level of the

483 adrenal SRN. Although it has been shown that a severe stressor can increase

484 cytokine levels in the brain and pituitary even in the absence of inflammation

485 (O'Connor K et al. 2003), and that ACTH can increase cytokine secretion in the

486 adrenal gland *in vitro* (Judd and MacLeod, 1992; Call GB et al. 2000), we did not see

487 such an increase in the level of adrenal cytokines following a high ACTH stimulation

488 alone.

489

490 A surprising finding of our study is the biphasic change in DAX-1 hnRNA, mRNA and

491 protein observed in the LPS experiment. While we know that IL-6 down-regulates

492 DAX-1 gene expression in bovine zona fasciculate cells, studies in different

493 steroidogenic tissues have shown that TNF-α can increase the expression of DAX-1

494 protein (Sadasivam 2015). Indeed, a rapid increase in TNF-α levels in plasma has

495 been observed shortly after LPS stimulation in the rat (Givalois, 1994), and we have

496 observed a rapid increase in TNF-α hnRNA and mRNA in this study. It is therefore

497 tempting to speculate that a transient enhancement of DAX-1 in response to

498 increased TNF-α may occur in the zona fasciculata of rats injected with LPS, prior to

499 the decrease induced by IL-6.

500

501 The sustained CORT response to transient ACTH following an LPS injection

502 suggests a disruption in the GR-mediated intra-adrenal feedback loop. This could be

503 a factor underlying the dissociated dynamics between ACTH and CORT observed in

504 stress scenarios. Uncovering the origin of this dissociated dynamics is key to

505 understanding a number of physiological and pathological conditions where

506 sustained high levels of CORT have been observed even after ACTH has returned to

507 normal (8). Consistent with this, our model predicts that cytokine effects on the DAX-

508 1 regulatory "hub" of the SRN may explain the dynamic dissociation between ACTH

509 and CORT during inflammation.

510

511 With regard to other measured factors that were not included in the model, on the

512 whole, we observed a dynamic activity that was consistent with the ACTH and/or

513 LPS stimulation. However, we did observe some discrepancies with previous studies;

514 for example, it has been shown that ACTH induces the expression of MC2R (Winnay

515 and Hammer, 2006). However, in our study we found that, while a small pulse of

516 ACTH increased MC2R hnRNA and mRNA, administration of LPS decreased MC2R

517 hnRNA and mRNA. Similarly, while a pulse of ACTH had no effect on HSL

518 expression, LPS decreased both HSL hnRNA and mRNA. This suggests that

519 inflammatory stress can lead to a decrease in ACTH signalling and cholesterol

520 availability, which may in turn lead to adrenal hypo-responsiveness in the longer-term

521 that is often observed in chronic inflammation and sepsis (Boonen et al. 2015).

522

523 In summary, we have presented a mathematical model of steroidogenesis that

524 makes qualitative predictions in response to a range of ACTH stimuli. Further *in vitro*

525 experiments are required to shed light on the specific molecular mechanisms

526 regulating the cross-talk between steroidogenic genes, which would enable us to

527 refine our models to make quantitative predictions. Nonetheless, we have shown that

528 our mathematical model of the adrenal SRN delivers valuable insight about the

19

529   transient and rapid adrenal dynamics observed in response to ACTH perturbations

530   during both basal and acute stress scenarios. In future work, the model could be

531   further exploited to study several ACTH-independent mechanisms of adrenal

532   sensitivity, such as splanchnic nerve-mediated effects on steroidogenesis (43), the

533   effect of metabolic factors such as leptin and insulin (6), and the effects on SRN

534   dynamics caused by acute and chronic exposure to synthetic glucocorticoids.

535

536   **Materials and Methods**

537

538   **Animals and surgery**

539   All experiments were conducted on adult male Sprague–Dawley rats (Harlan

540   Laboratories, Inc., Blackthorn, UK) weighting 220-250g at the time of arrival.

541   Rats were anaesthetised using isoflurane and an indwelling catheter was inserted in

542   the right jugular vein as previously described (44).

543

544   **Experiments and tissue collection**

545   All experiments started at 9 AM and were performed 5–7 days after the surgery. Rats

546   were given: *i*) an intravenous injection of synthetic ACTH (10 ng per 0.1 ml; *ACTH*

547   *pulse experiment); ii*) four sub-cutaneous injections of ACTH (2 µg/kg; *high dose*

548   *ACTH experiment; iii)* an intravenous injection of LPS (25 µg/rat in 0.1 mL of sterile

549   saline; *LPS experiment)*.

550

551   After decapitation, trunk blood was collected and plasma processed for ACTH and

552   corticosterone measurement as previously described (Spiga et al., 2007). Adrenal

553   glands were collected and the inner zones (comprising the *zona fasciculata* and the

554   *zona reticularis* of the cortex and the adrenal medulla) were separated from the outer

555   zone (containing the *zona glomerulosa* and the *capsula*). Individual inner zones were

556   immediately frozen until processing for isolation of RNA for real-time quantitative

557   polymerase chain reaction (RTqPCR; left adrenal), and for protein extraction for

558   Western immunoblotting and corticosterone measurement (right adrenal) as

559   previously described (38, 45).

560

561   **Statistical analysis**

562   Data were analyzed using the non-parametric Kruskal-Wallis Test. Statistical

563   significance was set at $P < 0.05$.

564

565   **Mathematical model**

566   We developed a mathematical model of the adrenal SRN that accounts for the time

567   evolution of core components of the full network, namely: A-CORT, pGR, and genes

568   DAX-1, SF-1, and StAR. The model postulates a network architecture based on

569   known biological interactions, with parameter values estimated from the literature

570   and calibrated using the ACTH i.v. pulse data. The network architecture and kinetic

571   parameter values remained invariant for generating predictions about the high s.c.

572   ACTH and LPS challenge experiments.

573

574   Because of the involvement of a slow genomic pathway and a fast non-genomic one,

575   we wrote the model in terms of a set of DDEs, where the delays were associated to

576   the gene transcription and translation processes. Our set of non-linear, coupled

577   DDEs was numerically integrated using XPPAUT (46) and PyDDE using a fixed time

578   step of 0.001 min and a 4th order Runge-Kutta integrator with adaptive steps. The

579   model development and complete set of model equations are detailed in the Supp.

580   Text.

581

582   More details on the materials and methods can be found in SI Appendix, Supp. Text.

583   Access to data, associated protocols, code, and materials is available upon

584   reasonable request.

585

Acknowledgments

586

587

591

Author contributions

592

593

594 FS, JJW, JRT and SLL designed research. FS and ZZ performed research. FS, EZ

595 and JJW analysed data. EZ and JJW developed and analysed mathematical models.

596 FS, EZ, and JJW wrote the paper with revision by all authors.

597

References

598

599

600 1. Ixart G, *et al.* (1994) Short-term but not long-term adrenalectomy
601 modulates amplitude and frequency of the CRH41 episodic release in
602 push-pull cannulated median eminence of free-moving rats. *Brain*
603 *research* 658(1-2):185-191.
604 2. Ixart G, Barbanel G, Nouguier-Soule J, & Assenmacher I (1991) A
605 quantitative study of the pulsatile parameters of CRH-41 secretion in
606 unanesthetized free-moving rats. *Exp Brain Res* 87(1):153-158.
607 3. Walker JJ, *et al.* (2012) The origin of glucocorticoid hormone oscillations.
608 *PLoS Biol* 10(6):e1001341.
609 4. Walker JJ, Terry JR, & Lightman SL (2010) Origin of ultradian pulsatility in
610 the hypothalamic-pituitary-adrenal axis. *Proc Biol Sci* 277(1688):1627-
611 1633.
612 5. Henley DE, *et al.* (2009) Development of an automated blood sampling
613 system for use in humans. *J Med Eng Technol* 33(3):199-208.
614 6. Bornstein SR, Engeland WC, Ehrhart-Bornstein M, & Herman JP (2008)
615 Dissociation of ACTH and glucocorticoids. *Trends Endocrinol Metab*
616 19(5):175-180.
617 7. Tkachenko IV, Jaaskelainen T, Jaaskelainen J, Palvimo JJ, & Voutilainen R
618 (2011) Interleukins 1alpha and 1beta as regulators of steroidogenesis in
619 human NCI-H295R adrenocortical cells. *Steroids* 76(10-11):1103-1115.
620 8. Gibbison B, *et al.* (2015) Dynamic pituitary-adrenal interactions in
621 response to cardiac surgery. *Crit Care Med* 43(4):791-800.

622   9.   Kraemer FB & Shen WJ (2002) Hormone-sensitive lipase: control of
623   intracellular tri-(di-)acylglycerol and cholesteryl ester hydrolysis. *Journal*
624   *of lipid research* 43(10):1585-1594.
625   10.   Lin D*, et al.* (1995) Role of steroidogenic acute regulatory protein in
626   adrenal and gonadal steroidogenesis. *Science* 267(5205):1828-1831.
627   11.   Caron KM*, et al.* (1997) Characterization of the promoter region of the
628   mouse gene encoding the steroidogenic acute regulatory protein.
629   *Molecular endocrinology* 11(2):138-147.
630   12.   Martin LJ, Boucher N, Brousseau C, & Tremblay JJ (2008) The orphan
631   nuclear receptor NUR77 regulates hormone-induced StAR transcription
632   in Leydig cells through cooperation with Ca2+/calmodulin-dependent
633   protein kinase I. *Molecular endocrinology* 22(9):2021-2037.
634   13.   Jo Y & Stocco DM (2004) Regulation of steroidogenesis and steroidogenic
635   acute regulatory protein in R2C cells by DAX-1 (dosage-sensitive sex
636   reversal, adrenal hypoplasia congenita, critical region on the X
637   chromosome, gene-1). *Endocrinology* 145(12):5629-5637.
638   14.   Carsia RV & Malamed S (1979) Acute self-suppression of
639   corticosteroidogenesis in isolated adrenocortical cells. *Endocrinology*
640   105(4):911-914.
641   15.   Loose DS, Do YS, Chen TL, & Feldman D (1980) Demonstration of
642   glucocorticoid receptors in the adrenal cortex: evidence for a direct
643   dexamethasone suppressive effect on the rat adrenal gland. *Endocrinology*
644   107(1):137-146.
645   16.   Peron FG, Moncloa F, & Dorfman RI (1960) Studies on the possible
646   inhibitory effect of corticosterone on corticosteroidogenesis at the
647   adrenal level in the rat. *Endocrinology* 67:379-388.
648   17.   Walker JJ*, et al.* (2015) Rapid intra-adrenal feedback regulation of
649   glucocorticoid synthesis. *Journal of the Royal Society, Interface / the Royal*
650   *Society* 12(102):20140875.
651   18.   Briassoulis G, Damjanovic S, Xekouki P, Lefebvre H, & Stratakis CA (2011)
652   The glucocorticoid receptor and its expression in the anterior pituitary
653   and the adrenal cortex: a source of variation in hypothalamic-pituitary-
654   adrenal axis function; implications for pituitary and adrenal tumors.
655   *Endocrine practice : official journal of the American College of*
656   *Endocrinology and the American Association of Clinical Endocrinologists*
657   17(6):941-948.
658   19.   Chong C*, et al.* (2017) Regulation of aldosterone secretion by
659   mineralocorticoid receptor-mediated signaling. *J Endocrinol.*
660   20.   Gummow BM, Scheys JO, Cancelli VR, & Hammer GD (2006) Reciprocal
661   regulation of a glucocorticoid receptor-steroidogenic factor-1
662   transcription complex on the Dax-1 promoter by glucocorticoids and
663   adrenocorticotropic hormone in the adrenal cortex. *Mol Endocrinol*
664   20(11):2711-2723.
665   21.   Babu PS*, et al.* (2002) Interaction between Dax-1 and steroidogenic
666   factor-1 in vivo: increased adrenal responsiveness to ACTH in the absence
667   of Dax-1. *Endocrinology* 143(2):665-673.
668   22.   Fan W*, et al.* (2004) Protein kinase A potentiates adrenal 4 binding
669   protein/steroidogenic factor 1 transactivation by reintegrating the
670   subcellular dynamic interactions of the nuclear receptor with its

671   cofactors, general control nonderepressed-
672   5/transformation/transcription domain-associated protein, and
673   suppressor, dosage-sensitive sex reversal-1: a laser confocal imaging
674   study in living KGN cells. *Mol Endocrinol* 18(1):127-141.

675   23.   Sugawara T*, et al.* (1997) Regulation of expression of the steroidogenic
676   acute regulatory protein (StAR) gene: a central role for steroidogenic
677   factor 1. *Steroids* 62(1):5-9.

678   24.   Sugawara T, Kiriakidou M, McAllister JM, Kallen CB, & Strauss JF, 3rd
679   (1997) Multiple steroidogenic factor 1 binding elements in the human
680   steroidogenic acute regulatory protein gene 5'-flanking region are
681   required for maximal promoter activity and cyclic AMP responsiveness.
682   *Biochemistry* 36(23):7249-7255.

683   25.   Winnay JN & Hammer GD (2006) Adrenocorticotropic hormone-mediated
684   signaling cascades coordinate a cyclic pattern of steroidogenic factor 1-
685   dependent transcriptional activation. *Molecular endocrinology* 20(1):147-
686   166.

687   26.   Carnes M, Brownfield MS, Kalin NH, Lent S, & Barksdale CM (1986)
688   Episodic secretion of ACTH in rats. *Peptides* 7(2):219-223.

689   27.   Carnes M, Kalin NH, Lent SJ, Barksdale CM, & Brownfield MS (1988)
690   Pulsatile ACTH secretion: variation with time of day and relationship to
691   cortisol. *Peptides* 9(2):325-331.

692   28.   Wang Z, Frederick J, & Garabedian MJ (2002) Deciphering the
693   phosphorylation "code" of the glucocorticoid receptor in vivo. *J Biol Chem*
694   277(29):26573-26580.

695   29.   Liu Y*, et al.* (2013) Transcriptional regulation of episodic glucocorticoid
696   secretion. *Molecular and cellular endocrinology* 371(1-2):62-70.

697   30.   Spiga F, Liu Y, Aguilera G, & Lightman SL (2011) Temporal effect of
698   adrenocorticotrophic hormone on adrenal glucocorticoid steroidogenesis:
699   involvement of the transducer of regulated cyclic AMP-response element-
700   binding protein activity. *J Neuroendocrinol* 23(2):136-142.

701   31.   Anthonsen MW, Ronnstrand L, Wernstedt C, Degerman E, & Holm C
702   (1998) Identification of novel phosphorylation sites in hormone-sensitive
703   lipase that are phosphorylated in response to isoproterenol and govern
704   activation properties in vitro. *J Biol Chem* 273(1):215-221.

705   32.   Ragazzon B*, et al.* (2006) Adrenocorticotropin-dependent changes in SF-
706   1/DAX-1 ratio influence steroidogenic genes expression in a novel model
707   of glucocorticoid-producing adrenocortical cell lines derived from
708   targeted tumorigenesis. *Endocrinology* 147(4):1805-1818.

709   33.   Zacharowski K*, et al.* (2006) Toll-like receptor 4 plays a crucial role in the
710   immune-adrenal response to systemic inflammatory response syndrome.
711   *Proceedings of the National Academy of Sciences of the United States of*
712   *America* 103(16):6392-6397.

713   34.   Givalois L*, et al.* (1994) Temporal cascade of plasma level surges in ACTH,
714   corticosterone, and cytokines in endotoxin-challenged rats. *Am J Physiol*
715   267(1 Pt 2):R164-170.

716   35.   Marketon JI & Sternberg EM (2010) The glucocorticoid receptor: a
717   revisited target for toxins. *Toxins (Basel)* 2(6):1357-1380.

718   36.   Bouazza B, *et al.* (2012) Cytokines alter glucocorticoid receptor
719   phosphorylation in airway cells: role of phosphatases. *Am J Respir Cell Mol*
720   *Biol* 47(4):464-473.
721   37.   Malek H, Ebadzadeh MM, Safabakhsh R, Razavi A, & Zaringhalam J (2015)
722   Dynamics of the HPA axis and inflammatory cytokines: Insights from
723   mathematical modeling. *Comput Biol Med* 67:1-12.
724   38.   Spiga F, *et al.* (2011) ACTH-dependent ultradian rhythm of corticosterone
725   secretion. *Endocrinology* 152(4):1448-1457.
726   39.   Achermann JC, Meeks JJ, & Jameson JL (2001) Phenotypic spectrum of
727   mutations in DAX-1 and SF-1. *Molecular and cellular endocrinology* 185(1-
728   2):17-25.
729   40.   Iyer AK & McCabe ER (2004) Molecular mechanisms of DAX1 action. *Mol*
730   *Genet Metab* 83(1-2):60-73.
731   41.   Zhao Y, *et al.* (2006) Zebrafish dax1 is required for development of the
732   interrenal organ, the adrenal cortex equivalent. *Molecular endocrinology*
733   20(11):2630-2640.
734   42.   Zazopoulos E, Lalli E, Stocco DM, & Sassone-Corsi P (1997) DNA binding
735   and transcriptional repression by DAX-1 blocks steroidogenesis. *Nature*
736   390(6657):311-315.
737   43.   Ulrich-Lai YM, Arnhold MM, & Engeland WC (2006) Adrenal splanchnic
738   innervation contributes to the diurnal rhythm of plasma corticosterone in
739   rats by modulating adrenal sensitivity to ACTH. *Am J Physiol Regul Integr*
740   *Comp Physiol* 290(4):R1128-1135.
741   44.   Spiga F, *et al.* (2007) Effect of the glucocorticoid receptor antagonist Org
742   34850 on basal and stress-induced corticosterone secretion. *Journal of*
743   *neuroendocrinology* 19(11):891-900.
744   45.   Park SY, *et al.* (2013) Constant light disrupts the circadian rhythm of
745   steroidogenic proteins in the rat adrenal gland. *Mol Cell Endocrinol* 371(1-
746   2):114-123.
747   46.   Ermentrout B (2002) *Simulating, analyzing, and animating dynamical*
748   *systems: a guide to XPPAUT for researchers and students* (Siam).
749
750
751
752
753
754

Figure legends

Figure 1. The simplified SRN represented in the mathematical model accounts

for both genomic and non-genomic processes occurring at different time

scales. Also considered in the model are the A-CORT/GR-mediated intra-adrenal feedback loop, and post-transcriptional and post-translational processes, including the ACTH-mediated stabilisation of StARp37.

Figure 2. The calibrated model reproduces the SRN dynamics following a short pulse of ACTH. Fitting the model to data successfully reproduced the rapid and transient synthesis of A-CORT **(a)** and GR activation **(b)**. The model also made qualitative predictions about the induction of DAX-1, SF-1, and StAR genes **(d-f)** that closely matched the *in vivo* data. Similarly, the model approximated the expression of the gene products, as judged from the dynamics of mRNA **(g-i)** and protein levels **(j-l)**. Red dashed lines indicate the time of ACTH injection. Representative Western immunoblotting images for pGR, StARp37, SF-1 and DAX-1 are shown in SI Appendix, Fig. S3.
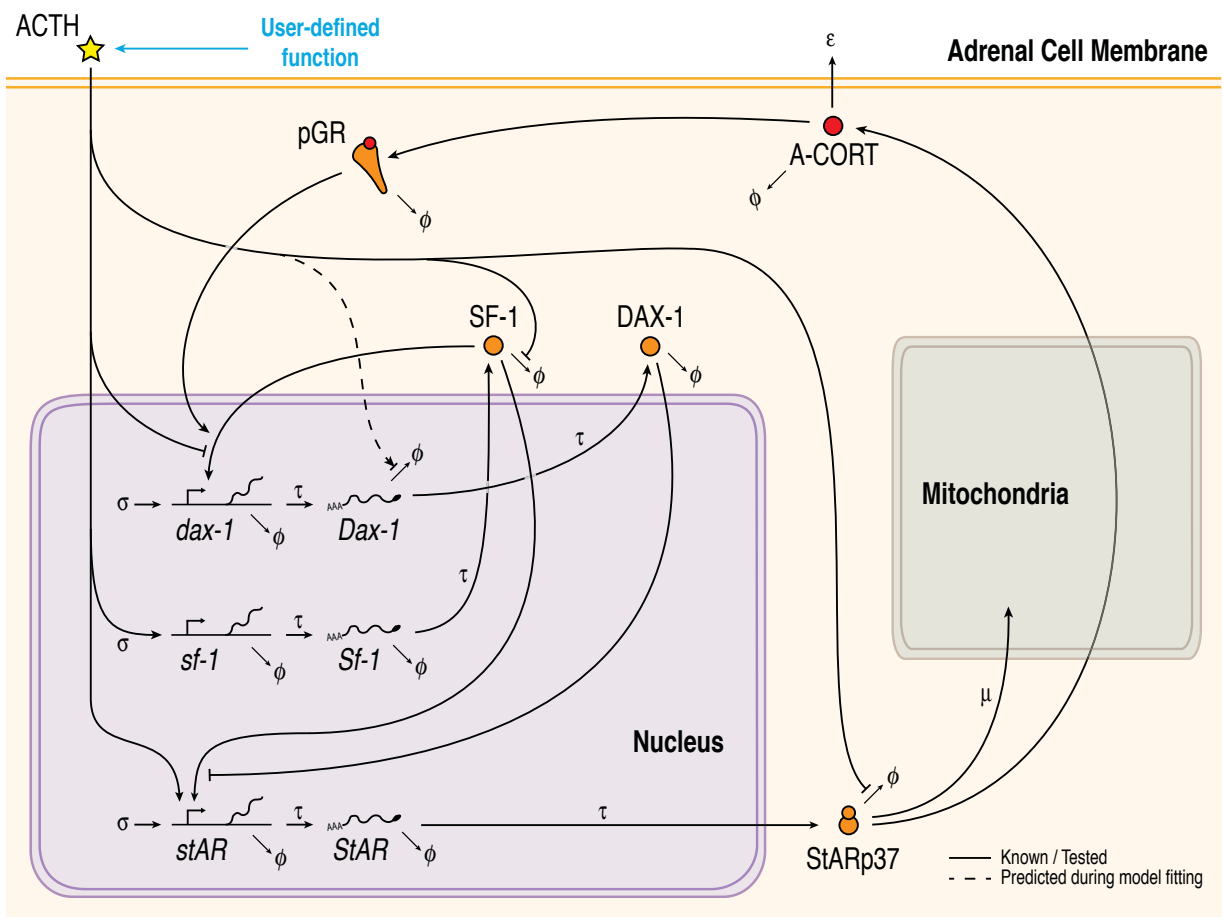
Figure 3. The model reproduces the SRN dynamics following a high dose of ACTH. The model successfully reproduced the long and transient surges of A-CORT **(a)** and GR activation **(b)**. The model also made qualitative predictions about the induction of DAX-1, SF-1, and StAR genes **(d-f)** that closely matched the *in vivo* data. Similarly, the model approximated the expression of the gene products, as judged from the dynamics of mRNA **(g-i)** and protein levels **(j-l)**. Red dashed lines indicate the time of ACTH injections. Representative Western immunoblotting images for pGR, StARp37, SF-1 and DAX-1 are shown in Fig. SI Appendix, S5.
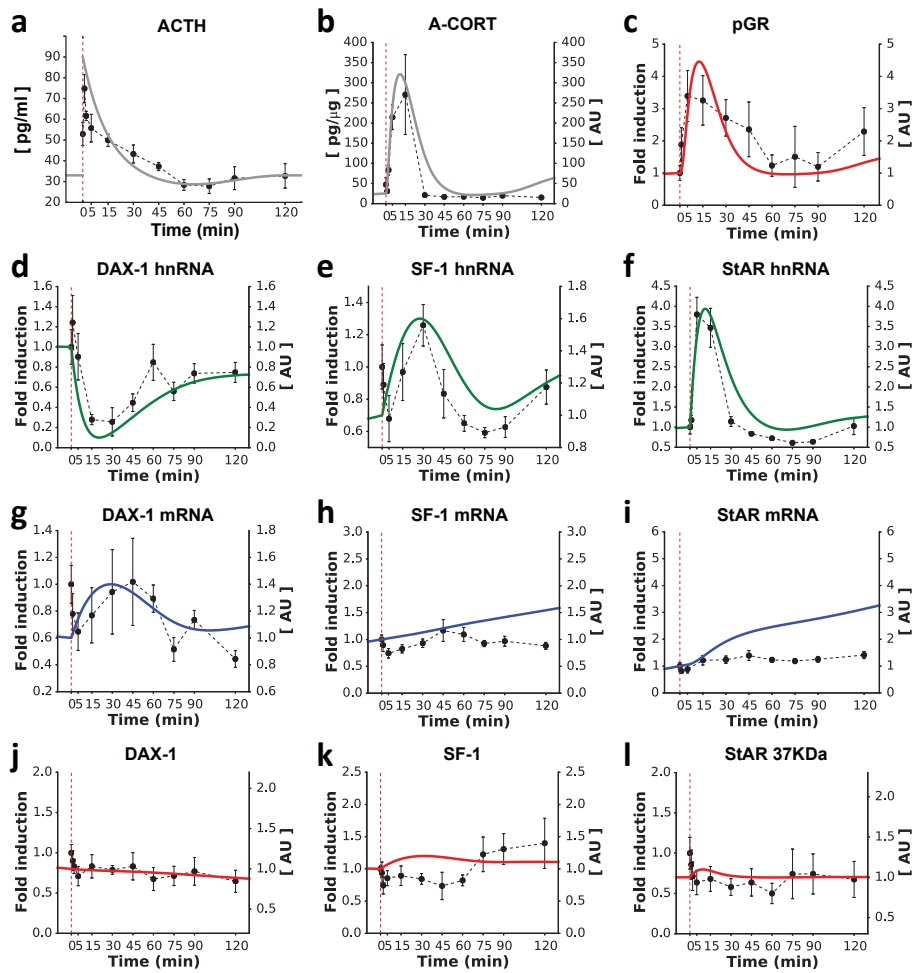
Fig. 4. Before considering the cross-talk with the immune pathway, the model partially reproduces the dynamic effects of an LPS-induced pulse of ACTH on components of the SRN. While ignoring cytokine effects, the model successfully reproduced the long and sustained surge of A-CORT **(a)**, but not of GR activation
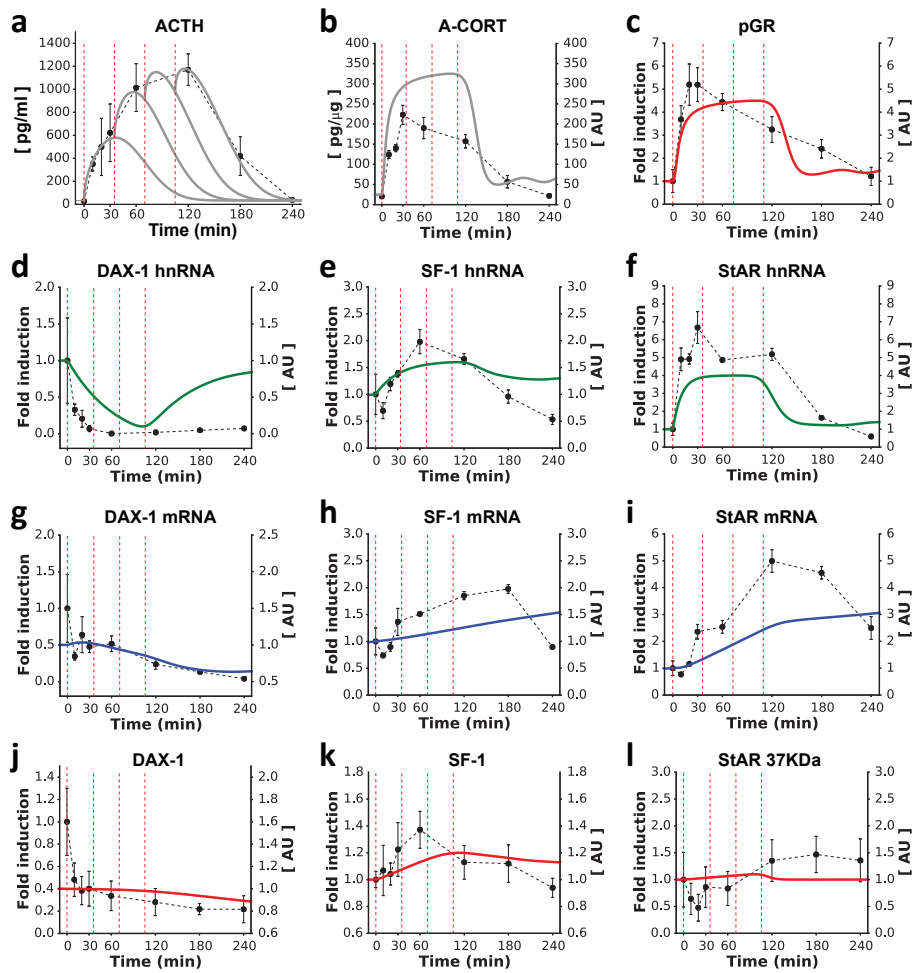
(b). The model also made qualitative predictions about the gene expression dynamics that closely matched the DAX-1 *in vivo* data **(d, g, j)**, but failed to reproduce the SF-1 **(e, h, k)** and StAR **(f, i, l)** gene expression dynamics. Red dashed lines indicate the time of LPS injection. Representative Western immunoblotting images for pGR, StARp37, SF-1 and DAX-1 are shown in SI Appendix, Fig. S6.
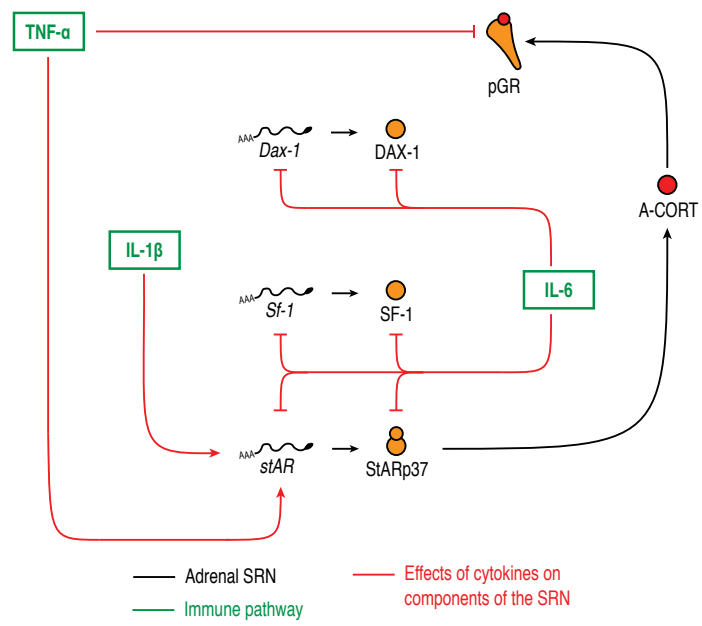
Fig. 5. Cytokine effects upon targets within the adrenal SRN considered in the model. The transient cytokine pulses elicited by LPS were used as additional input functions to ACTH.
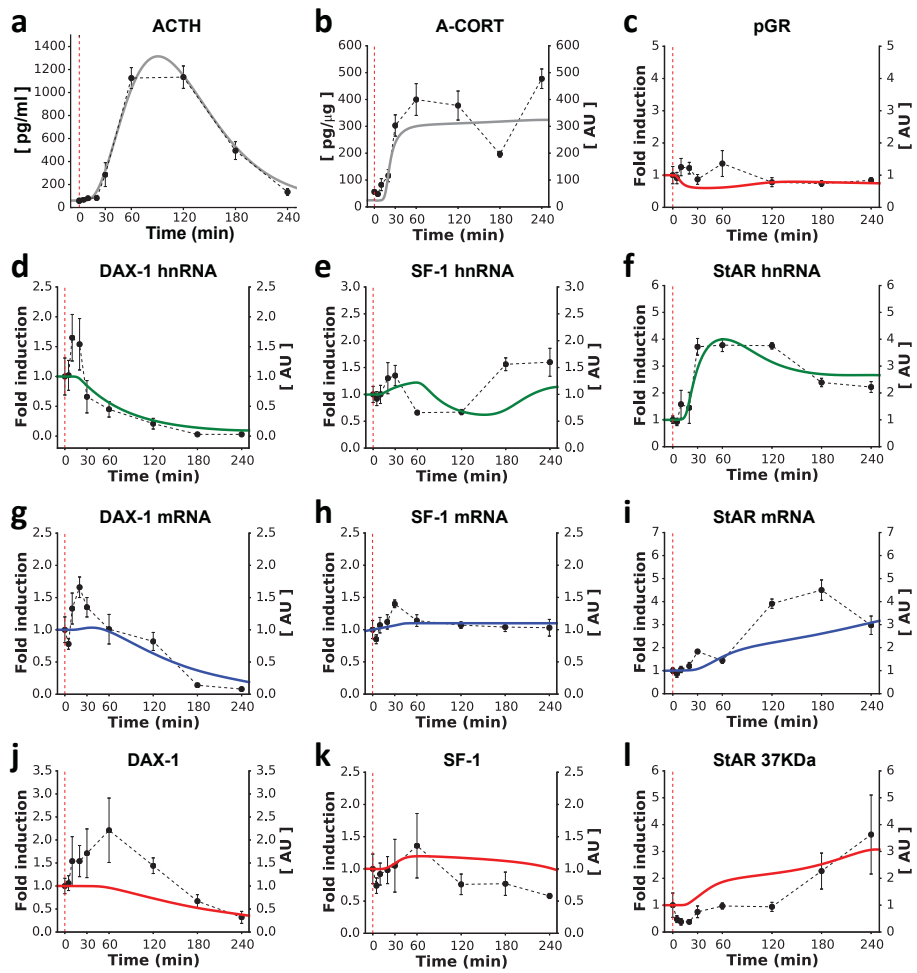
Figure 6. The extended model reproduces the SRN dynamics following administration of LPS. After accounting for cytokine effects, the model successfully reproduced the long and sustained surge of A-CORT **(a)** and approximated the pGR dynamics **(b)**. The model also made qualitative predictions about the transient induction of DAX-1, SF-1, and StAR genes **(d-f)** that approximated the *in vivo* data. Similarly, the model approximated the expression of the gene products, as judged from the dynamics of mRNA **(g-i)** and protein levels **(j-l)**. Red dashed lines indicate the time of LPS injection. Representative Western immunoblotting images for pGR, StARp37, SF-1 and DAX-1 are shown in SI Appendix, Fig. S6.
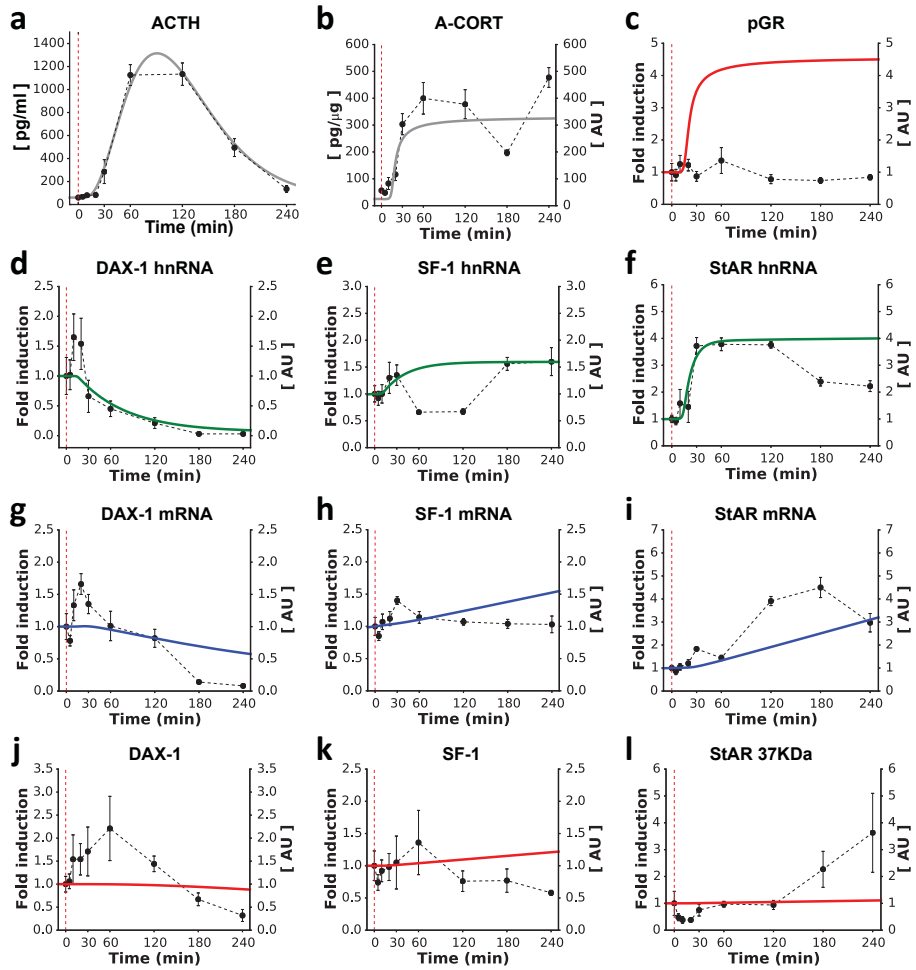
a ACTH

b A-CORT

c pGR

d DAX-1 hnRNA

e SF-1 hnRNA

f StAR hnRNA

g DAX-1 mRNA

h SF-1 mRNA

i StAR mRNA

j DAX-1

k SF-1

l StAR 37KDa

TNF-α

pGR

AAA Dax-1 → DAX-1

A-CORT

IL-1β

IL-6

AAA Sf-1 → SF-1

AAA stAR → StARp37

——— Adrenal SRN

——— Effects of cytokines on
components of the SRN

——— Immune pathway
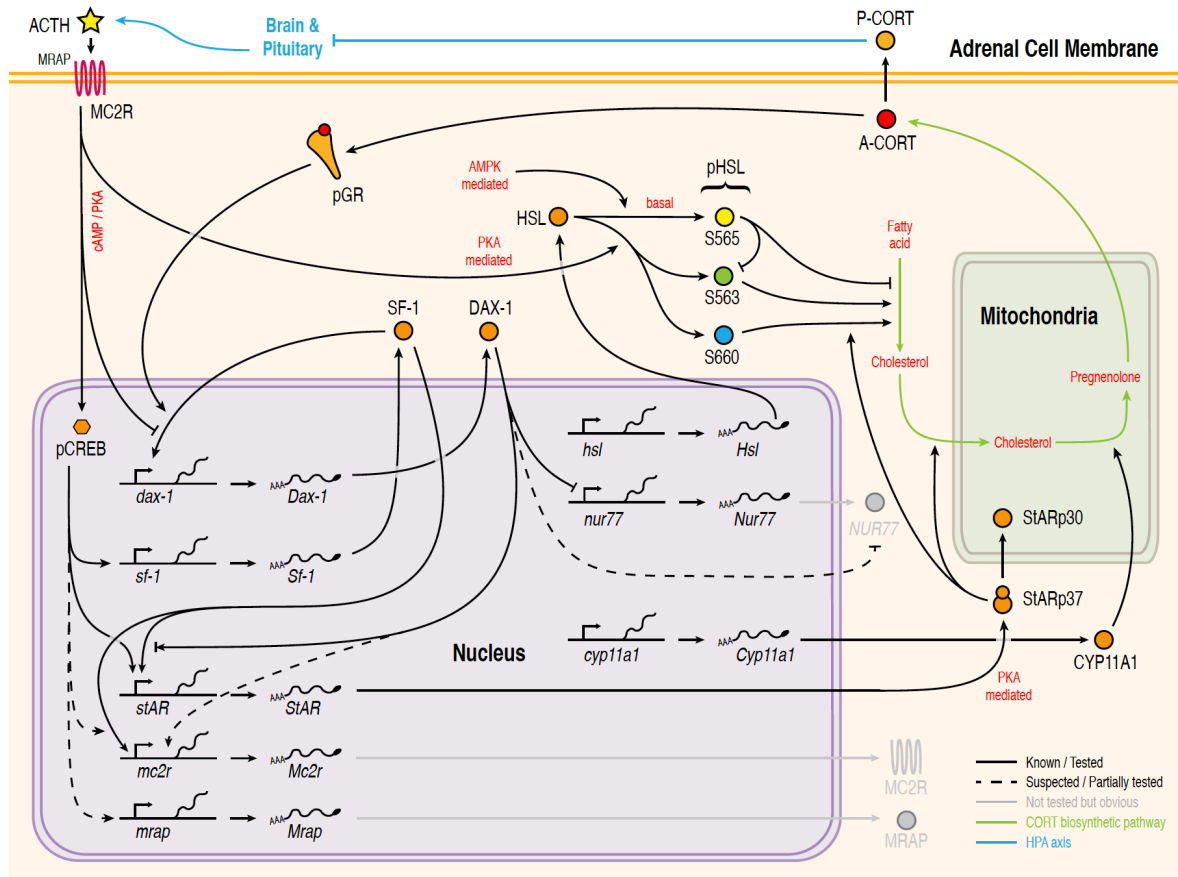
SI Appendix

Supplementary Figures

Fig. S1. The steroidogenic regulatory network (SRN). The synthesis of glucocorticoids in adrenocortical cells is governed at multiple levels by both genomic and non-genomic components. In addition to the high degree of cross-talk between these components, an intra-adrenal feedback loop mediated by A-CORT/GR may underlie adrenal responsiveness and maintain appropriate levels of glucocorticoids.
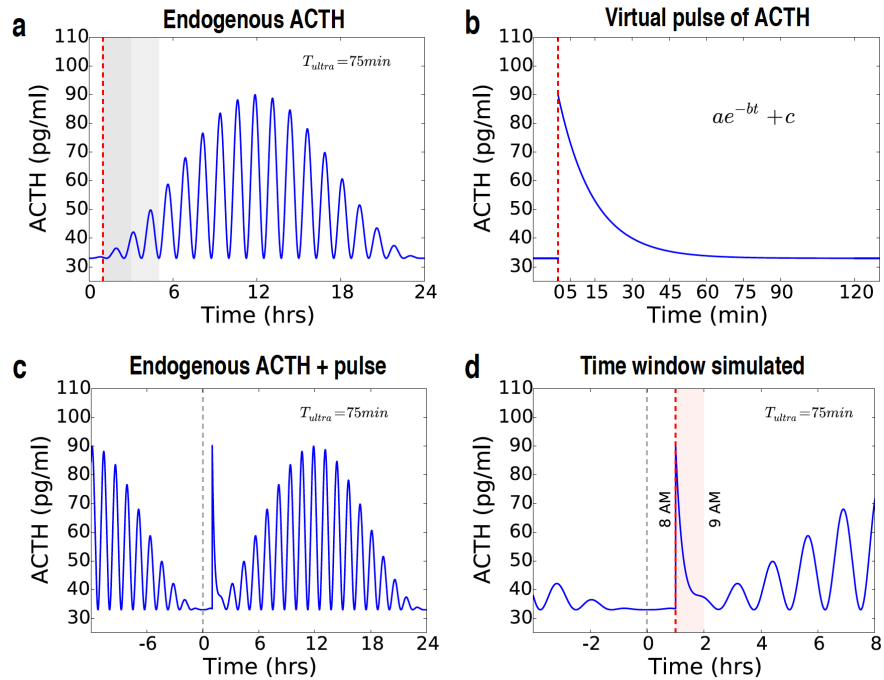
a Endogenous ACTH

$T_{ultra} = 75min$

b Virtual pulse of ACTH

$ae^{-bt} + c$

c Endogenous ACTH + pulse

$T_{ultra} = 75min$

d Time window simulated

8 AM   9 AM

$T_{ultra} = 75min$

Fig. S2. Virtual (*in silico*) computer simulations of ACTH endogenous oscillations and perturbations. (a) The model was driven by oscillating levels of ACTH that represented endogenous fluctuations. **(b)** A simple function representing a "virtual" pulse of ACTH. **(c)** The pulse was of a size comparable to the maximum endogenous levels in normal physiological conditions. **(d)** The "virtual" pulse was given near the nadir of the circadian ACTH rhythm, at approximately the same time corresponding to the *in vivo* experiments (between 8 and 9 AM).
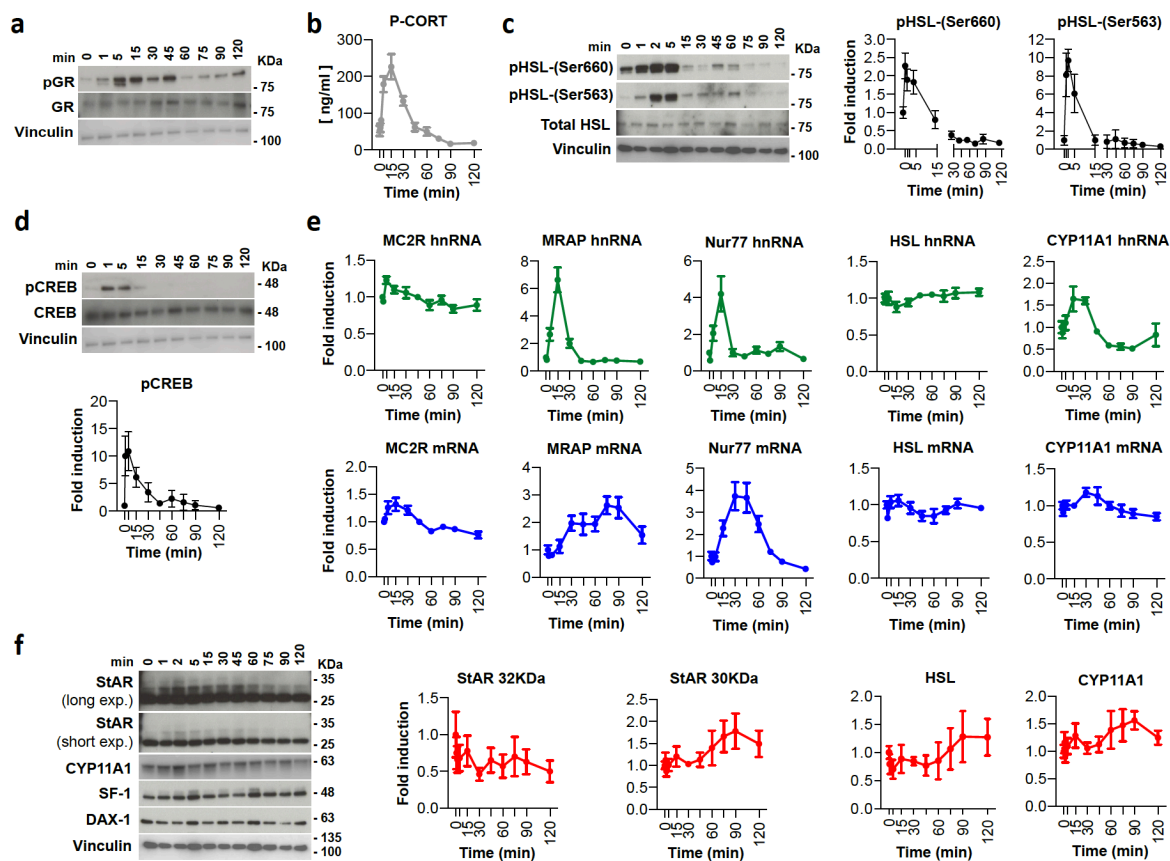
Fig. S3. A short pulse of ACTH dynamically activates the SRN and CORT biosynthesis. (a) Representative Western immunoblotting of the effect of a pulse of ACTH on intra-adrenal phospho-GR (quantification is shown in Fig. 2c in the main text). **(b)** A pulse of ACTH dynamically affects plasma CORT (P-CORT). **(c)** Representative Western immunoblotting and quantification of the dynamic effect of a pulse of ACTH on phosphorylation of HSL (pHSL-(Ser660) and pHSL-(Ser563)). **(d)** Representative Western immunoblotting and quantification of the dynamic effect of a pulse of ACTH on phosphorylation of CREB in Ser133. **(e)** A pulse of ACTH dynamically affects plasma CORT steroidogenic genes hnRNA and mRNA. **(f)** Representative Western immunoblotting and quantification of the dynamic effect of a pulse of ACTH on steroidogenic protein expression (quantification of StARp37, SF-1 and DAX-1 proteins is shown in Fig. 2 in the main text). For Western immunoblotting data, optical density was normalised to Vinculin; for RTqPCR, data were normalised to GAPDH mRNA levels; Western immunoblotting and RTqPCR data are expressed as fold induction of time 0 (n=4-7/time point). Details of asymptotic significances are reported in Table S2.
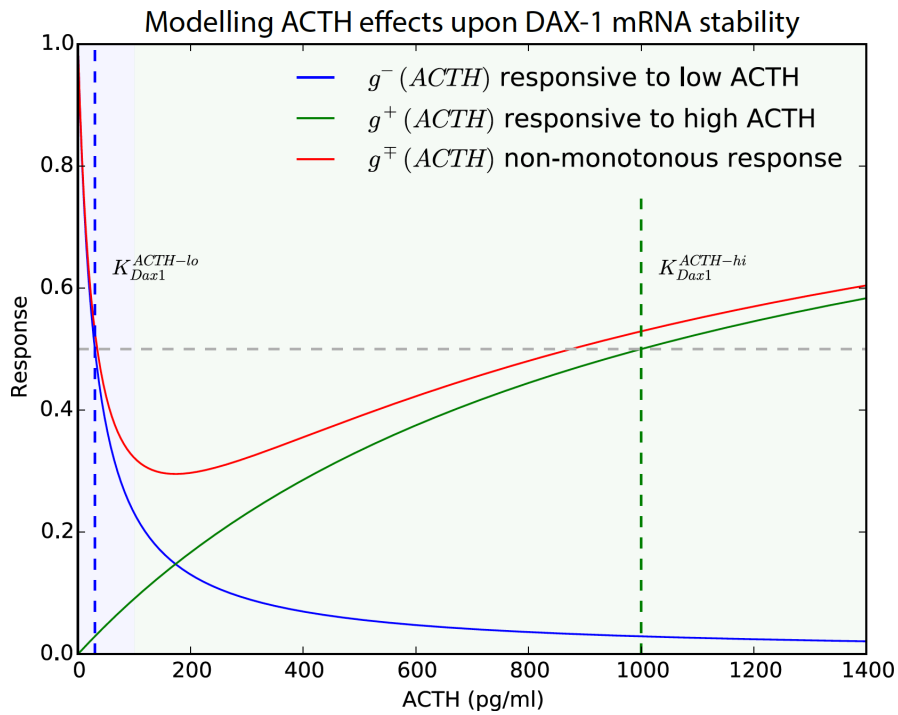
Fig. S4. Modelling ACTH dose-dependent effects on DAX-1 mRNA stability. While an increasing function g$^+$ is supported by previous experiments performed at high doses of ACTH, only a decreasing function g$^-$ fits our *in vivo* experiments at low doses of ACTH. We hypothesise a non-monotonous –decreasing, then increasing– response mechanism that successfully reproduces our data at both low and high doses of ACTH.
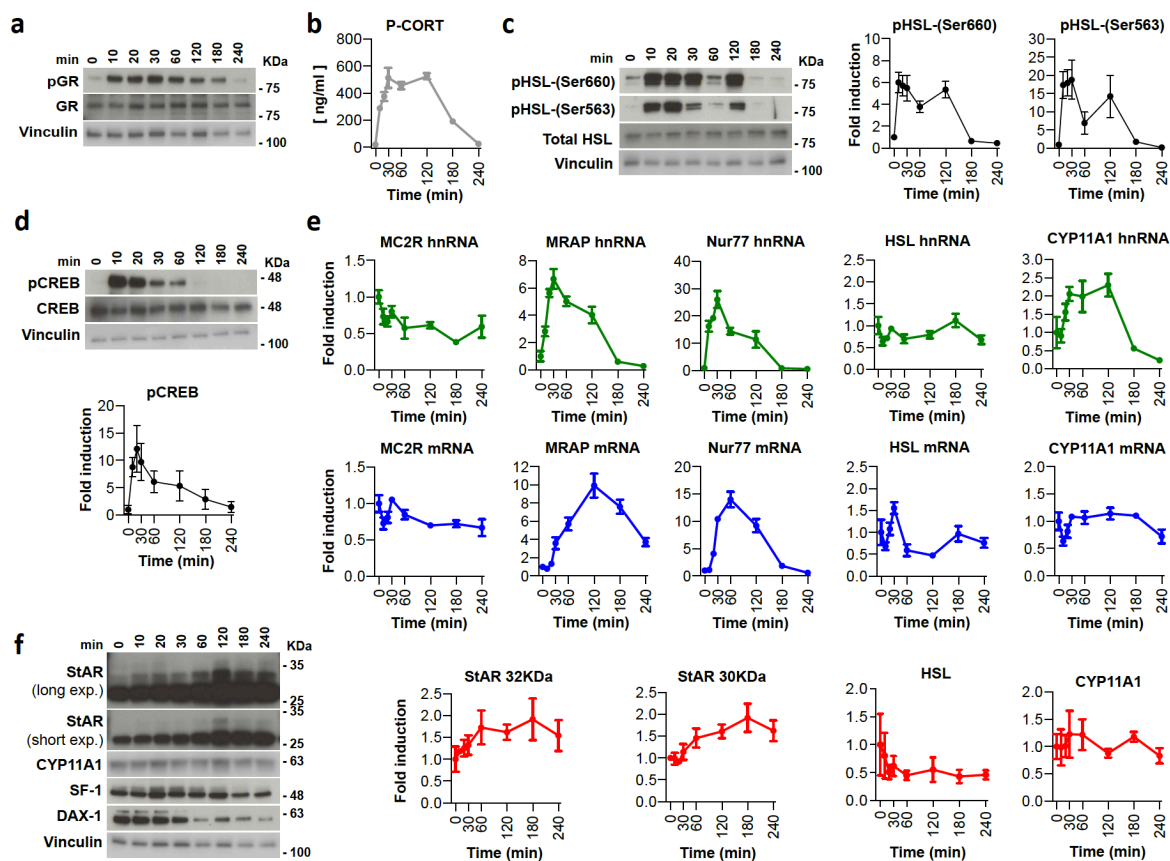
Fig. S5. Dynamic synthesis of adrenal glucocorticoids and activity of the SRN following a high dose of ACTH. (a) Representative Western immunoblotting of the effect of a high dose of ACTH on intra-adrenal phospho-GR (quantification is shown in Fig. 3c in the main text). **(b)** A high dose of ACTH dynamically affects plasma CORT (P-CORT). **(c)** Representative Western immunoblotting and quantification of the dynamic effect of a high dose of ACTH on phosphorylation of HSL (pHSL-(Ser660) and pHSL-(Ser563)). **(d)** Representative Western immunoblotting and quantification of the dynamic effect of a high dose of ACTH on phosphorylation of CREB in Ser133. **(e)** A high dose of ACTH dynamically affects plasma CORT steroidogenic genes hnRNA and mRNA. **(f)** Representative Western immunoblotting and quantification of the dynamic effect of a high dose of ACTH on steroidogenic protein expression (quantification of StARp37, SF-1 and DAX-1 proteins is shown in Fig. 3 in the main text). For Western immunoblotting data, optical density was normalised to Vinculin; for RTqPCR, data were normalised to GAPDH mRNA levels; Western immunoblotting and RTqPCR data are expressed as fold induction of time 0 (n=4/time point). Details of asymptotic significances are reported in Table S2.
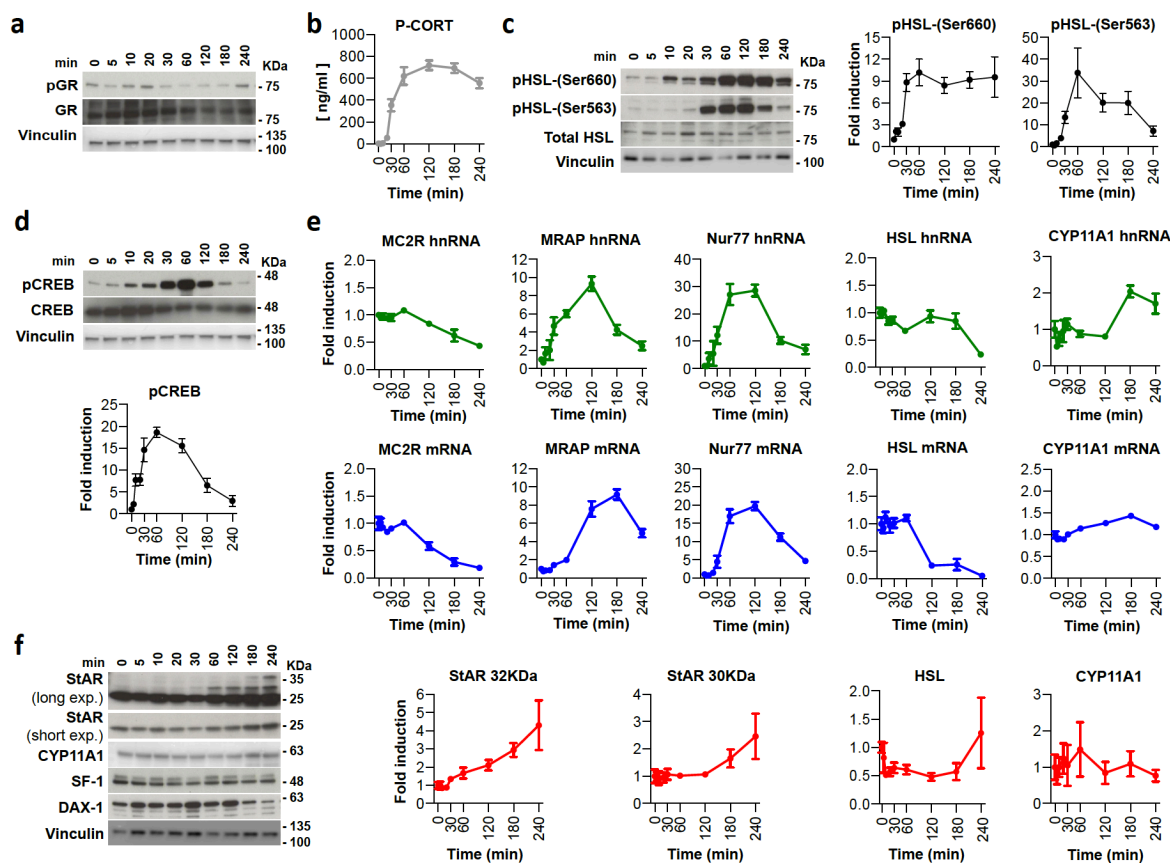
Fig. S6. Dynamic synthesis of adrenal glucocorticoids and activity of the SRN following administration of LPS. (a) Representative Western immunoblotting of the effect of LPS on intra-adrenal phospho-GR (quantification is shown in Fig. 4c in the main text). **(b)** Administration of LPS dynamically affects plasma CORT (P-CORT). **(c)** Representative Western immunoblotting and quantification of the dynamic effect of LPS on phosphorylation of HSL (pHSL-(Ser660) and pHSL-(Ser563)). **(d)** Representative Western immunoblotting and quantification of the dynamic effect of LPS on phosphorylation of CREB in Ser133. **(e)** Administration of LPS dynamically affects plasma CORT steroidogenic genes hnRNA and mRNA. **(f)** Representative Western immunoblotting and quantification of the dynamic effect of LPS on steroidogenic protein expression (quantification of StARp37, SF-1 and DAX-1 proteins is shown in Fig. 4 in the main text). For Western immunoblotting data, optical density was normalised to Vinculin; for RTqPCR, data were normalised to GAPDH mRNA levels; Western immunoblotting and RTqPCR data are expressed as fold induction of time 0 (n=4-12/time point). Details of asymptotic significances are reported in Table S2.
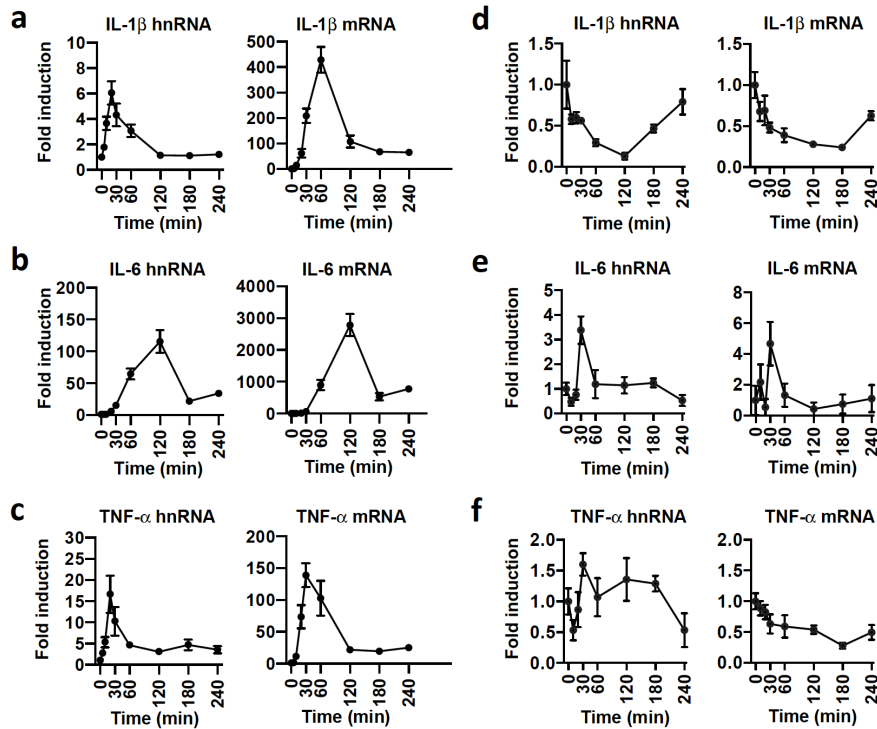
Fig. S7. Effect of LPS vs direct administration of a high dose of ACTH on intra-adrenal cytokines gene expression. The effect of LPS and high s.c. ACTH was evaluated by measuring the hnRNA and mRNA dynamics by RTqPCR (n=4-5/time point). Data are expressed as fold induction of time 0. LPS administration dynamically increased **(a)** IL-1β hnRNA (P<0.0001) and mRNA (P<0.0001), **(b)** IL-6 hnRNA (P<0.0001) and mRNA (P<0.0001), and **(c)** TNF-α hnRNA (P=0.006) and mRNA (P<0.0001). In contrast, administration of a high dose of ACTH significant decreased **(d)** IL-1β hnRNA (P=0.005) and mRNA (P=0.003), whereas only a small but significant increase was observed in **(e)** IL-6 hnRNA (P=0.03) but not on mRNA (P=0.171), and a trend toward significant increase and a significant decrease was observed in **(f)** TNF-α hnRNA (P=0.067) and mRNA (P=0.02), respectively.
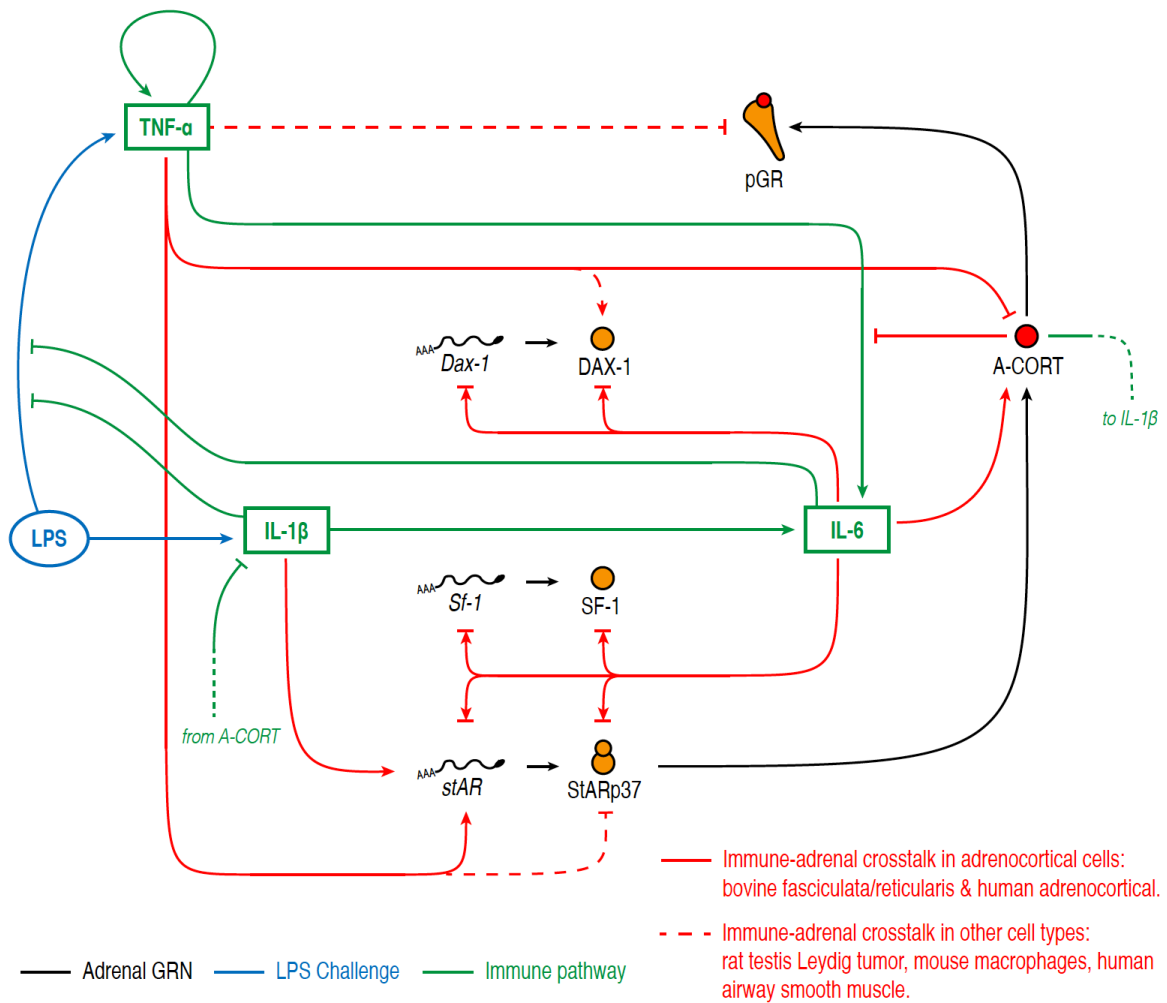
Fig. S8. Cross-talk between the SRN and the immune pathway. During the inflammatory response elicited by LPS, the synthesis of glucocorticoids in adrenocortical cells is modulated by the immune pathway through cytokines. The SRN, in turn, also feeds back upon these cytokines, thus exhibiting cross-talk between both regulatory networks.
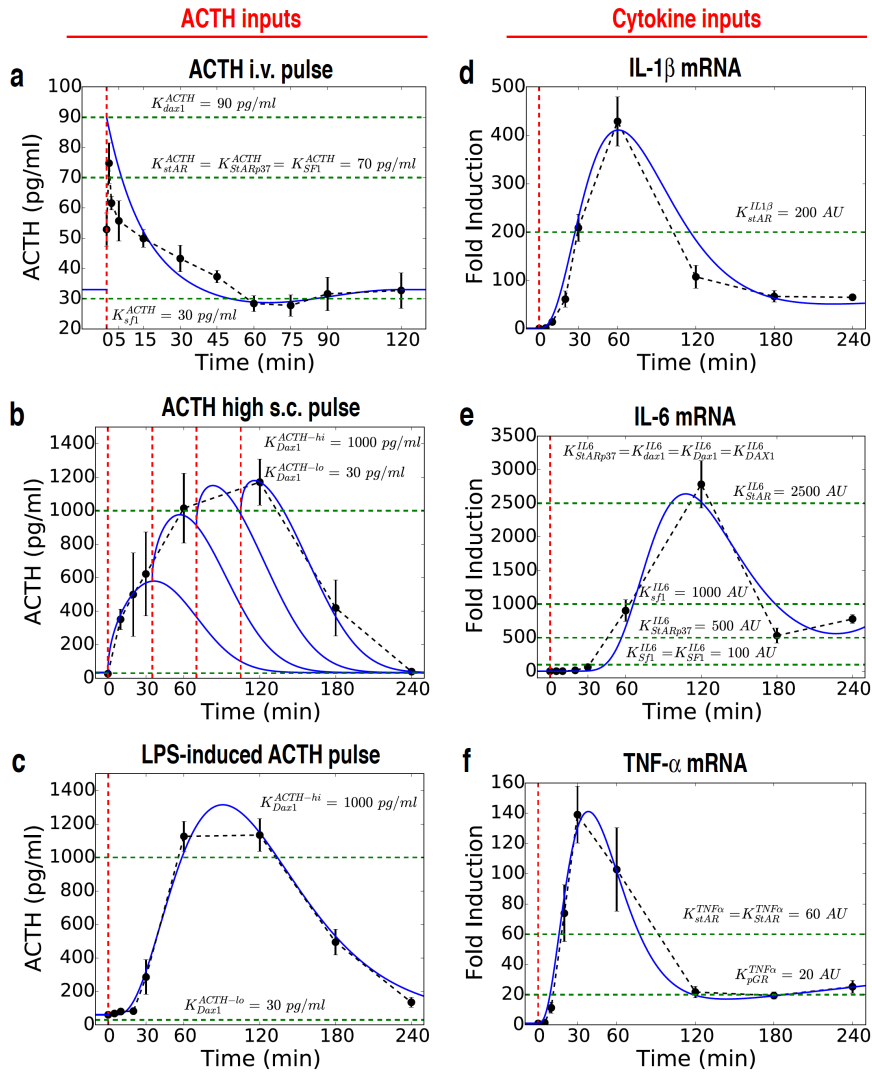
ACTH inputs

a ACTH i.v. pulse

$K_{daz1}^{ACTH} = 90\ pg/ml$

$K_{stAR}^{ACTH} = K_{StARp37}^{ACTH} = K_{SF1}^{ACTH} = 70\ pg/ml$

$K_{sf1}^{ACTH} = 30\ pg/ml$

b ACTH high s.c. pulse

$K_{Dax1}^{ACTH-hi} = 1000\ pg/ml$

$K_{Dax1}^{ACTH-lo} = 30\ pg/ml$

c LPS-induced ACTH pulse

$K_{Dax1}^{ACTH-hi} = 1000\ pg/ml$

$K_{Dax1}^{ACTH-lo} = 30\ pg/ml$

Cytokine inputs

d IL-1β mRNA

$K_{stAR}^{IL1\beta} = 200\ AU$

e IL-6 mRNA

$K_{StARp37}^{IL6} = K_{daz1}^{IL6} = K_{Dax1}^{IL6} = K_{DAX1}^{IL6}$

$K_{StAR}^{IL6} = 2500\ AU$

$K_{sf1}^{IL6} = 1000\ AU$

$K_{StARp37}^{IL6} = 500\ AU$

$K_{Sf1}^{IL6} = K_{SF1}^{IL6} = 100\ AU$

f TNF-α mRNA

$K_{stAR}^{TNF\alpha} = K_{StAR}^{TNF\alpha} = 60\ AU$

$K_{pGR}^{TNF\alpha} = 20\ AU$

Fig. S9. ACTH and cytokine "virtual" pulse input functions used in the computer simulations and their associated sensitivities. (a) Small pulse (low dose) of ACTH, **(b)** large pulse of ACTH integrated by four cumulative doses, **(c)** large pulse of ACTH elicited by LPS, **(d-f)** cytokine pulses elicited by LPS.

Supplementary Tables

Supplementary Table 1. Primer Sequences.

Target	Forward Primer	Reverse Primer
CYP11A1 hnRNA	TGTGTGTGTGACCCCAGGAGAC	CCCAGGTCCTGCTTGAGAGGCT
CYP11A1 mRNA	TGCGAGGGTCCTAACCCGGA	ACCTTCCAGCAGGGGCACGA
DAX-1 hnRNA	TCCAGGCCATCAAGAGTTTC	AAGCTCACCCACTTGACCAC
DAX-1 mRNA	TCCAGGCCATCAAGAGTTTC	GTGCTCAGTGAGGATCTGC
GAPDH mRNA	CCATCACTGCCACCCAGAAGA	GACACATTGGGGGTAGGAACA
HSL hnRNA	AGGTAGGAGCTGTACCCCTG	CTGCAAAGACGTTGGACAGC
HSL mRNA	TATCCGCTCTCCGGTTGA	CGAGCACTGGAGGAGTGTTT
IL-1β hnRNA	AGTTGTCCGTGTGTATGGGATG	GCCAGGCAGAAAGGTTTTTGTT
IL-1β mRNA	ACCTATGTCTTGCCCGTGGA	AGGTCGTCATCATCCCACGA
IL-6 hnRNA	CCCAGAGCACTCCACAAGG	TCTTGGTCCTTAGCCACTCCT
IL-6 mRNA	AGCCACTGCCTTCCCTACTT	GCCATTGCACAACTCTTTTCTCA
MC2R hnRNA	GAAGTCCGTGAGGTTGSACA	TTGTGCGGAAGGATCCAGTTT
MC2R mRNA	GCTTTTGATCCCTGCTTTGAGTG	CATCTGTTAAAGAAGGAAAGGCTGG
MRAP hnRNA	ACCTCATTCCTGTGGACGAG	ACCCGCCATATTATCACTGC
MRAP mRNA	CCTCCCGGTGTGTGGCCTCT	GGGGACTATGCCTTACCTGTGGGG
NR4A1 hnRNA	CTTGTGGGGTCCCTGCCTGC	ACGTGGAGAAGGGGCGGTCT
NR4A1 mRNA	GCGGAACCGCTGCCAGTTCT	GCATCTGGGGGCTGCTTGGG
SF-1 hnRNA	AGAGGGTGATGGGCTGCT	ACCTCCACCAGGCACAATAG
SF-1 mRNA	CGCCAGGAGTTTGTCTGTCT	ACCTCCACCAGGCACAATAG
StAR hnRNA	GCAGCAGCAACTGCAGCACTAC	GTGCCCCCGGAGACTCACCT
StAR mRNA	CTGGCAGGCATGGCCACACA	GGCAGCCACCCCTTGAGGTC
TNF-α hnRNA	CCGTGACTGTAATCGCCCTAC	CTTTAGGAGGCTGCAGAGAGAC
TNF-α mRNA	AAATGGGCTCCCTCTATCAGTTC	TCTGCTTGGTGGTTTGCTACGAC

Supplementary Table 2. Statistical information (P values). Related to Figs. 2–4, 6, and to Figs. S3,5,6.

Component	P value		
	Fig. 2 and Fig. S3	Fig. 3 and Fig. S5	Figs. 4, 6 and Fig. S6
ACTH	<0.0001	0.002	<0.0001
A-CORT	<0.0001	<0.0001	<0.0001
P-CORT	<0.0001	<0.0001	<0.0001
pHSL-(Ser660)	<0.0001	0.001	<0.0001
pHSL-(Ser563)	<0.0001	0.003	<0.0001
pCREB	0.001	0.028	<0.0001
StAR hnRNA	<0.0001	0.001	<0.0001
StAR mRNA	0.067	<0.0001	<0.0001
CYP11A1 hnRNA	<0.0001	0.002	0.007
CYP11A1 mRNA	0.013	0.051	<0.0001
MRAP hnRNA	<0.0001	<0.0001	<0.0001
MRAP mRNA	<0.0001	<0.0001	<0.0001
MC2R hnRNA	0.016	0.051	0.002
MC2R mRNA	<0.0001	0.002	<0.0001
HSL hnRNA	0.517	0.16	0.006
HSL mRNA	0.221	0.021	<0.0001
Nur77 hnRNA	<0.0001	<0.0001	<0.0001
Nur77 mRNA	<0.0001	<0.0001	<0.0001
SF-1 hnRNA	0.008	0.003	0.005
SF-1 mRNA	0.361	0.002	0.091
DAX-1 hnRNA	0.001	0.001	0.001
DAX-1 mRNA	0.154	0.002	<0.0001
StARp37	0.755	0.441	<0.0001
StARp32	0.967	0.457	<0.0001
StARp30	0.354	0.007	0.433
CYP11A1	0.482	0.814	0.971
HSL	0.777	0.993	0.146
SF-1	0.385	0.492	0.76
DAX-1	0.728	0.301	0.003
pGR	0.032	0.003	0.528

Supplementary Materials and Methods

Animals

All experiments were conducted on adult male Sprague–Dawley rats (Harlan Laboratories, Inc., Blackthorn, UK) weighting 220-250g at the time of arrival. Animals were given a 1-week acclimatization period prior to the start of the experiments, they were maintained under a 14 h light, 10 h dark schedule (lights on at 0500 h), and housed four per cage with ad libitum access to food and water. All animal procedures were approved by the University of Bristol Ethical Review Group and were conducted in accordance with Home Office guidelines and the United Kingdom Animals (Scientific Procedures) Act, 1986.

Surgery

Rats were anaesthetised using isoflurane and an indwelling catheter was inserted in the right jugular vein as previously described (Spiga et al., 2007). In brief, the right jugular vein was exposed, and a silastic-tipped (Merck, Whitehouse, NJ) polythene cannula (Portex, Hythe, UK) was inserted into the vessel to allow substance infusion. Cannula was prefilled with pyrogen-free heparinized (10 IU/ml) isotonic saline; the free end was exteriorized through a scalp incision and then tunnelled through a protective spring that was anchored to the parietal bones using two stainless steel screws and self-curing dental acrylic. For the high dose ACTH experiment, in addition to the intravenous cannula, during the same surgery a subcutaneous cannula was implanted under the skin between the shoulder blades. After recovery, animals were housed in individual cages in a soundproof room. The end of the protective spring was attached to a mechanical swivel that rotated through 360° in a horizontal plane and 180° through a vertical plane, allowing the rats to maximize freedom of movement. The cannula was flushed daily with heparinized saline to maintain patency.

Experiments and tissue collection

All experiments started at 9 AM and were performed 5–7 days after the surgery. *ACTH pulse experiment.* To investigate the dynamic adrenal response to an ACTH pulse rats were given an intravenous injection of synthetic ACTH (10 ng per 0.1 ml, i.v.; Synachten, Alliance Pharma, Cheltenam, United Kingdom). *High dose ACTH experiment.* To investigate the effect of a high dose of ACTH, that is able to produce similar plasma ACTH levels as observed after LPSs treatment, rats were given four injections of ACTH (2 µg/kg, sc; Synachten Depot, AlliancePharma, Cheltenam, United Kingdom) at 35-minute intervals, as previously described in (Gibbison et al., 2015). *LPS experiment.* To investigate the dynamic

adrenal response to an inflammatory stress rats were given an intravenous injection of LPS (Escherichia coli, clone 055:B5; 25 μg/rat in 0.1 mL of sterile saline; Sigma, Dorset, United Kingdom).

At the end of each experiment, rats were overdosed with 0.2 mL of sodium pentobarbitone (Euthatal, 200 mg/mL; Merial, Harlow, United Kingdom) at specific time points shown in the figures. Trunk blood was collected in ice-cold tubes containing EDTA (0.5 M; pH 7.4) and Trasylol (Aprotinin, 500,000 KIU/mL, Roche Diagnostics). Plasma was separated by centrifugation and then stored at –80°C until processed for ACTH and corticosterone measurement.

Adrenal glands were collected and the inner zones (comprising the *zona fasciculata* and the *zona reticularis* of the cortex and the adrenal medulla) were separated from the outer zone (containing the *zona glomerulosa* and the *capsula*). Individual inner zones were immediately frozen until processing for isolation of RNA for real-time quantitative polymerase chain reaction (RTqPCR; left adrenal), and for protein extraction for Western immunoblotting and corticosterone measurement (right adrenal) as previously described (Park et al., 2013; Spiga et al., 2011b).

RNA isolation and RT-qPCR

Total RNA was extracted from the inner zone of individual adrenals using TRIzol reagent (Invitrogen, Hopkinton, MA, USA), followed by purification using RNeasy mini kit reagents, and column DNase digestion (Qiagen, Valencia, CA, USA) to remove genomic DNA contamination. Complementary DNA was reverse transcribed from 1 μg of total RNA using Cloned AMV First-Strand cDNA synthesis kit (Invitrogen). Primers were designed to specifically detect primary transcript (hnRNA) or mRNA (Table S1). Fast SYBRGreen Master (Applied Biosystems, Foster City, CA, USA) was used for the amplification mixture with each primer at a final concentration of 200 nm and 2 μl of cDNA for a total reaction volume of 25 μl. PCR reactions were performed on a spectrofluorometric thermal cycler. The expression of each target gene was normalized to glyceraldehyde 3-phosphate dehydrogenase (GAPDH) mRNA as determined in a separate real-time PCR reaction. The absence of RNA detection when the reverse transcription step was omitted indicated the lack of genomic DNA contamination in the RNA samples.

Western immunoblotting

Whole cell lysate from the inner zone of individual adrenals were prepared using RIPA buffer (Sigma) supplemented with 0.2 mM Na orthovanadate, 2 mM NaF, and Complete Protease

Inhibitor (Roche Diagnostics Ltd., Burgess Hill, UK). Protein concentration was quantified by spectrophotometry using the Pierce BCA protein assays, (Thermo Fisher Scientific Inc. Rockford, IL, USA). Aliquots of each sample (10–15 µg of protein) were loaded and separated in a 10% or 4–15% Tris–Glycine gel (BioRad, Hercules, CA, USA), transferred to a PVD membrane (GE Amersham Biosciences, Piscataway, NJ, USA), blocked with 5% non-fat milk or 1% bovine serum albumin (BSA, sigma) in 1 × Tris-buffered saline plus 0.05% Tween 20 (TBST) and incubated overnight with Aliquots of each sample (10–15 µg of protein) were loaded and separated in a 10% or 4–15% Tris–Glycine gel (BioRad, Hercules, CA, USA), transferred to a PVD membrane (GE Amersham Biosciences, Piscataway, NJ, USA), blocked with 5% non-fat milk or 1% bovine serum albumin (BSA, sigma) in 1 × Tris-buffered saline plus 0.05% Tween 20 (TBST) and incubated overnight with antibodies to StAR, DAX-1, CYP11A1, HSL, GR (Santa Cruz Biotechnologies, Inc., Dallas, TX, US), SF-1 (Upstate Biotechnlogies Inc., Lake Placid, NY, US); CREB, phospho-CREB(Ser133), phospho-HSL(Ser660), phospho-HSL(Ser563); phospho-GR(Ser211) (Cell Signalling Technology, Danvers, MA, US).

After washing with TBST, the membranes were incubated with a horseradish peroxidase-conjugated donkey anti-rabbit IgG or donkey anti-goat IgG (Santa Cruz Biotechnologies). Immunoreactive bands were visualized using ECL Plus TM reagents (GE Amersham Biosciences) followed by exposure to BioMax MR film (Eastman Kodak; Rochester, NY, USA). After film exposure, blots were stripped and assayed for anti-goat vinculin (Santa Cruz Biotechnology). The intensity of the protein targets bands integrated with the area was quantified using a computer image analysis system, Image J (developed at the National Institutes of Health and freely available at: http://rsb.info.nih.gov). Data points for each gene were then normalized relative to the vinculin band in the respective sample.

Hormone measurement
Adrenal CORT was measured in adrenal whole cell extract prepared for Western blotting and CORT levels were normalized to the total protein content. Total plasma and adrenal CORT was measured by radioimmunoassay (RIA) using a citrate buffer (pH 3.0) to denature the binding globulin as previously described (Spiga et al., 2007). Antiserum was kindly supplied by Professor Gabor Makara (Institute of Experimental Medicine, Budapest, Hungary) and [125I] CORT was purchased from Izotop (Budapest, Hungary). ACTH in plasma was measured by RIA using a commercially available assay (MP Biomedicals, Santa Ana, California, USA) in accordance with the manufacturer's instructions.

Statistics

Sample sizes in each experiment were determined on the basis of pilot studies and previous experience with similar experimental design. Animals were allocated to each experimental group (time point after treatment) by simple randomization. Experimenters were blinded to the experimental group at the time of hormones, RNA and protein measurements.

Data are represented as the mean ± SEM, hnRNA, mRNA and protein data are expressed as fold induction of basal (time 0). No animals or samples were excluded from statistical analysis. To check data for normality and equality of variance, we used Shapiro-Wilk and Leven tests, respectively. The overall effect of treatments was analysed using the Independent-Samples Kruskal-Wallis Test. Asymptotic significances for each experiment are shown in Table S2. Statistical significance was set at $P < 0.05$.

Mathematical Model

Contents

1 Model Development

The adrenal SRN controlling the CORT biosynthetic pathway is very complex (Fig. S1). In order to develop a useful yet, manageable mathematical model, we simplified the network by reducing the number of components to a minimum (Fig. 1). Our model predictions support these gene components as the core regulatory clockwork of the SRN. A list of source references to the connections between nodes in both the full and reduced network is shown in Table A.

The mathematical model is representative of a single adrenocortical cell stimulated by an ACTH input. Specifically, ACTH stimulates adrenocortical cells for controlling the biosynthesis of CORT, which, respectively, represent the 'input' and 'output' of the SRN. Since our model is decoupled from other components of the HPA axis, we reproduced endogenous ACTH levels originated from the brain by using an ultradian oscillatory input (T = 75 min) with circadian modulated amplitude. Thus, in basal, non-stressed conditions, the model dynamics is not static but exhibits an ultradian and circadian rhythmicity driven by the ACTH input. Some model assumptions and biological considerations are the following:

i) The model doesn't focus on the specifics of the CORT biosynthetic pathway within the mitochondria or its release into the bloodstream. Instead, we consider A-CORT as a better readout of the network since its increase occurs earlier than P-CORT, thus reflecting the very first product of CORT biosynthesis.

ii) The network architecture emphasises the crosstalk between StAR, DAX-1 and SF-1 genes. For each of these genes, their hnRNA, mRNA and protein species are modelled explicitly. Though MC2R, MRAP, Nur77 and HSL genes are included in the full network map (Fig. S1), the network architecture suggests they're not directly involved in feedback regulation within the genomic pathway.

iii) Likewise, even though the dynamics of the different phosphorylation states of the HSL protein (pHSL-S565, pHSL-S563 and pHSL-S660) is important to understand cholesterol synthesis, it is StARp37 the one controlling the mitochondrial import of cholesterol, which is the rate-limiting step for ACORT biosynthesis. Accordingly, we didn't include the pHSL dynamics in the present model.

iv) To decouple the intra-adrenal system from the whole HPA axis, we assumed ACTH as an externally controlled input that targets specific components within the adrenal SRN. This took the form of either an endogenous ultradian input with circadian amplitude, a single pulse perturbation, or a combination of both.

Furthermore, we simplified the model by reducing the number of model equations. For instance, cAMP, PKA and pCREB intermediary species in the signalling cascade ending in promoter regulation are not modelled explicitly. Though pCREB is known to regulate transcription of StAR [Manna et al., 2009; Sugawara et al., 1997a,b; Zhao et al., 2005] as well as of other steroidogenic genes, the components of the cascade are known to be downstream of the ACTH pathway, which is already considered in the model.

To reproduce experimental conditions, we administered "virtual" ACTH pulses near the circadian nadir of the endogenous ACTH oscillations. Specifically, we simulated 7 pulses, one every 10 min, distributed between 8 AM and 9 AM of the day. The dynamics during the 120 min following the stimuli was recorded and averaged for the ACTH i.v. pulse experiments, and during 240 min for the high s.c. ACTH and LPS challenge experiments.

1.1 DAX-1 Gene Expression

The dynamics of gene activation, represented by the newly synthesised, non-edited hnRNA $dax1$[1], can be represented by the following equation:

$$\dot{dax1} = \sigma_{dax1} + k_{dax1}f_{dax1}(SF1, pGR)g^{-}_{dax1}(ACTH) - \gamma_{dax1}dax1 \tag{1}$$

where σ_{dax1} is the basal transcription rate, k_{dax1} is the maximum transcription rate, γ_{dax1} is the $dax1$ hnRNA degradation rate, and f_{dax1} is a function accounting for $dax1$ transcription initiation by the synergistic action of SF1 and pGR, which is modulated by ACTH. Since the specific molecular mechanisms governing the Dax1[2] promoter activation are still poorly understood, we take an heuristic approach and propose a phenomenological function that captures the effects observed in the study by [Gummow et al., 2006], in which SF1 and GR were cotransfected with a Dax1-Luc reporter into JEG3 cells and stimulated with varying doses of dexamethasone (thus mimicking steroid activation of the GR). Subsequently, a similar experiment was performed in Y1 cells which were concomitantly stimulated with ACTH to assess the level of induction when SF1 and GR were present separately or simultanouesly.

CORT-activated GR, which we measured via its phosphorylated form pGR, is known to synergise with SF1 to enhance Dax1 gene expression (up to 30-fold activation in a dose-dependent dexamethasone stimulation experiment). In addition, SF1 is known to also activate the promoter in a pGR-independent way (11-fold activation). Moreover, Glucocorticoid Responsive Elements (GREs) have been identified in the Dax1 promoter and they are dose-responsive to dexamethasone stimulation in the absence of SF1 [Gummow et al., 2006]. However, we will not consider SF1-independent effects on f_{dax1} as the elicited fold activation is not only very close to baseline but also small when compared against SF1-pGR synergistic activation and SF1-dependent induction. Further experiments performed by [Gummow et al., 2006] suggest that SF1 and pGR form a molecular complex at the Dax1 promoter which enhances its expression upon steroid stimulation. Considering this and the role that SF1 has in regulating the expression of the StAR gene after binding to the DAX1 protein (thus forming another molecular complex) [Sugawara et al., 1997a,b; Fan et al., 2004; Gummow et al., 2006; Manna et al., 2009], we propose that f_{dax1} takes the form:

$$f_{dax1}(SF1, pGR) = \frac{\frac{SF1}{K_{SF1}} + \frac{SF1 \cdot pGR}{K_{SF1} \cdot K_G}}{1 + \frac{SF1}{K_{SF1}} + \frac{SF1 \cdot pGR}{K_{SF1} \cdot K_G}} \tag{2}$$

In Eq. 2, it can be seen that SF1 is necessary for activating the Dax1 promoter, either independently (i.e. in its free form) or forming a complex with pGR. Thus, pGR can be viewed as an enhancer which acts upon Dax1 promoter through the SF1-pGR complex. The non-linearity observed in Eq. 2 is expected from the pGR-independent SF1 binding to any of its three binding sites within the Dax1 promoter and from the synergy between the central SF1 binding site and the proximal GRE binding site that enhances expression [Gummow et al., 2006]. As the specific mechanisms of regulation are unknown, we chose the simplest empirical representation of the Dax1 promoter regulation by SF1 and pGR transcription factors.

Furthermore, [Gummow et al., 2006] also show that both the SF1 and SF1-pGR synergistic activation of the Dax1 promoter are decreased upon ACTH stimulation. We modelled this by multiplying the second term in Eq. 1 by a decreasing function $g^{-}_{dax1}(ACTH)$. As the specific mechanisms and molecular intermediaries of ACTH-dependent modulation are unknown, it is convenient to choose a non-linear Hill type function (see Eq. 3). The K's in Eqs. 1 and 2 account for half-maximum constants which were determined by fitting the model to data.

$$g^{-}_{dax1}(ACTH) = \frac{K^{ACTH^4}_{dax1}}{K^{ACTH^4}_{dax1} + ACTH^4} \tag{3}$$

---

[1]The hyphen in *dax-1*, *Dax-1*, *DAX-1*, *sf-1*, *Sf-1*, *SF-1*, and *A-CORT* labels was dropped to avoid confusion with a minus sign.

[2]In what follows, the non-italicised nomenclature will be used for gene names unless otherwise specified, whereas the italicised will be reserved for state variables used in the mathematical model (e.g. *dax1*, *Dax1*, and *DAX1* refer, respectively, to hnRNA, mRNA, and protein concentrations).

The mature transcript dynamics is given by

$$\dot{Dax1} = k_{Dax1}dax1_{\tau_{Dax1}} - \gamma_{Dax1}Dax1 \cdot g_{Dax1}^{\mp}(ACTH) \tag{4}$$

where k_{Dax1} stands for the mRNA maturation rate and γ_{Dax1} is the mRNA degradation rate. RT-PCR experiments aimed at detecting hnRNA can't distinguish the transcriptional stage at which the RNA is within the nucleus. However, we know that edition processes such as splicing have finished once mature mRNAs are detected. Hence, we assumed Eq. 4 is delayed by τ_{Dax1}, which accounts for the elapsed time since transcription initiation up to the emergence of a hnRNA plus the maturation time after completion of transcription (splicing, capping, polyadenylation and mRNA nuclear export processes).

In addition, high doses of ACTH are known to destabilise $Dax1$ transcripts [Ragazzon et al., 2006], which in a first instance was modelled by multiplying the turnover term in Eq. 4 by a positively increasing function of ACTH ($g_{Dax1}^{+}(ACTH)$). However, when re-calibrating the model by fitting it to our ACTH i.v. pulse experiments, we observed a mismatch between its predictions and our DAX1 mRNA and protein data. We realised that our assumption of a monotonously-increasing function was based on experimental results by [Ragazzon et al., 2006] that were performed using very high levels of ACTH. Thus, to fit our model to data from low ACTH i.v. pulse experiments, but keeping consistency with previous observations by [Ragazzon et al., 2006] at high ACTH levels, we hypothesised an ACTH dose-dependent control mechanism of $Dax1$ mRNA stability that was modelled assuming its turnover rate is modulated by the function $g_{Dax1}^{\mp}(ACTH)$. Though it's not clear how ACTH actually promotes or inhibits degradation of $Dax1$, we propose that a non-monotonous regulatory function would provide the best fit of the model to our experimental data in both the low and high ACTH *stimuli* experiments. We model this through a decreasing-then-increasing function containing two half-maximum constants: $K_{Dax1}^{ACTH-lo}$ for inhibition at low doses of ACTH, and $K_{Dax1}^{ACTH-hi}$ for activation at high doses of ACTH (Fig. S4). This function takes the form:

$$g_{Dax1}^{\mp}(ACTH) = \frac{K_{Dax1}^{ACTH-lo}}{K_{Dax1}^{ACTH-lo} + ACTH} + \frac{ACTH}{K_{Dax1}^{ACTH-hi} + ACTH} \tag{5}$$

Finally, the DAX1 protein dynamics is governed by:

$$\dot{DAX1} = k_{DAX1}Dax1_{\tau_{DAX1}} - \gamma_{DAX1}DAX1 \tag{6}$$

where k_{DAX1} stands for the protein translation rate, τ_{DAX1} is the delay associated to translation, and γ_{DAX1} is the protein degradation rate.

1.2   SF-1 Gene Expression

The dynamics of gene activation, represented by the newly synthesised, non-edited $sf1$ hnRNA, can be represented by the following equation:

$$\dot{sf1} = \sigma_{sf1} + k_{sf1}g_{sf1}^{+}(ACTH) - \gamma_{sf1}sf1 \tag{7}$$

where σ_{sf1} is the basal transcription rate, k_{sf1} is the maximum transcription initiation rate, and γ_{sf1} is the $sf1$ degradation rate. To the best of our knowledge, the SF1 gene is not subject to transcriptional regulation by any of the proteins considered in the model. Thus, conversely to Eq. 1, here we have no function accounting for $sf1$ transcription modulation by any transcription factors other than the effects induced by ACTH. This is modelled by a function $g_{sf1}^{+}(ACTH)$, which takes the form:

$$g_{sf1}^{+}(ACTH) = \frac{ACTH^4}{K_{sf1}^{ACTH^4} + ACTH^4} \tag{8}$$

Though in our model we consider that SF1 gene expression is regulated by ACTH alone [Ragazzon et al., 2006], regulation by other transcription factors within the steroidogenic pathway cannot be ruled out. This poses interesting questions about the role of this gene in controlling the adrenal

response. Moreover, evidence suggests that its mRNA and protein levels remain constant after variations in cAMP concentration, which is a known mediator of the ACTH pathway [Fan et al., 2004].

The mature transcript dynamics is given by:

$$\dot{Sf1} = k_{Sf1}sf1_{\tau_{Sf1}} - \gamma_{Sf1}g_{Sf1}(Sf1) \tag{9}$$

where k_{Sf1} stands for the mRNA maturation rate and γ_{Sf1} is the mRNA degradation rate. By similar arguments as in Eq. 4, we assumed Eq. 9 is delayed by τ_{Sf1}. Importantly, we found out that the best fit of the model to our data was achieved when assuming a Michaelis-Menten degradation of $Sf1$ mRNA. Thus, the function $h_{Sf1}(Sf1)$ takes the form:

$$h_{Sf1}(Sf1) = \frac{Sf1}{K_{Sf1} + Sf1} \tag{10}$$

Finally, the $SF1$ protein dynamics is governed by:

$$\dot{SF1} = k_{SF1}Sf1_{\tau_{SF1}} - \gamma_{SF1}SF1 \cdot g_{SF1}^-(ACTH) \tag{11}$$

where k_{SF1} stands for the protein translation rate, τ_{SF1} is the delay associated to translation, and γ_{SF1} is the protein degradation rate. Since ACTH is suspected to stabilise $SF1$, probably through phosphorylation or ubiquitination of the proteasome [Æsøy et al., 2002], we assume its turnover rate is modulated by a function $g_{SF1}^-(ACTH)$, which takes the form:

$$g_{SF1}^-(ACTH) = \frac{K_{SF1}^{ACTH}}{K_{SF1}^{ACTH} + ACTH} \tag{12}$$

1.3 StAR Gene Expression

The dynamics of StAR gene activation, represented by the newly synthesised, non-edited $stAR$ hnRNA, can be represented by the equation:

$$\dot{stAR} = \sigma_{stAR} + k_{stAR}f_{stAR}(SF1, DAX1)g_{stAR}^+(ACTH) - \gamma_{stAR}stAR \tag{13}$$

where σ_{stAR} is the basal transcription rate, k_{stAR} is the maximum transcription initiation rate, γ_{stAR} is the $stAR$ degradation rate, and f_{stAR} is a function accounting for $stAR$ transcription initiation controlled positively by $SF1$ and negatively by $DAX1$. This $DAX1$-mediated steroidogenic inhibition follows from the finding that $DAX1$ inhibits $SF1$ transactivation upon binding it [Babu et al., 2002; Fan et al., 2004], thus preventing StAR gene activation. In addition, ACTH is known to control the StAR gene activation directly through pCREB [Sugawara et al., 1997a,b; Manna et al., 2009]. However, since we're not modelling pCREB explicitly, we employ the function $g_{stAR}^+(ACTH)$ to model the StAR gene activation by ACTH. This function takes the form:

$$g_{stAR}^+(ACTH) = \frac{ACTH^4}{K_{stAR}^{ACTH^4} + ACTH^4} \tag{14}$$

In summary, an $SF1$ dependent activation mechanism, similar to the one modelled in Eq. 2, has been shown to be responsible for StAR gene activation [Sugawara et al., 1997b; Manna et al., 2003; Fan et al., 2004; Xu et al., 2009]. This follows from cotransfection experiments carried out by [Fan et al., 2004] to explore the effects of $SF1$ (a.k.a. Ad4BP) and $DAX1$ concomitantly with Forskolin stimulation of the PKA pathway.

These considerations were taken into account to assume that f_{stAR} takes the form:

$$f_{stAR}(SF1, DAX1) = \frac{\frac{SF1}{K_{SF1}}}{1 + \frac{SF1}{K_{SF1}} + \frac{DAX1}{K_D}} \tag{15}$$

In Eq. 13, it can be seen that both ACTH and $SF1$ are necessary for activating $stAR$, whereas $DAX1$ modulates the promoter activity by binding to $SF1$ at the promoter site (the gene is inactive

5

if either ACTH or $SF1$ are absent, but not if $DAX1$ is). Importantly, this empirical approach facilitates modifying Eq. 15 if we wish to account for $DAX1$ dosage dependent effects observed in diseased states [Xu et al., 2009; Sadasivam et al., 2015]. Just as in Eq. 2, the K's in Eq. 15 account for half-maximum constants (often interpreted as sensitivities) and were determined by fitting the model to data.

The mature transcript dynamics is given by:

$$\dot{StAR} = k_{StAR} stAR_{\tau_{StAR}} - \gamma_{StAR} h_{StAR}(StAR) \tag{16}$$

where k_{StAR} stands for the mRNA maturation rate and γ_{StAR} is the mRNA degradation rate. By similar arguments as in Eq. 4, we assumed Eq. 16 is delayed by τ_{StAR}. Importantly, we found out that the best fit of the model to data was achieved when assuming a Michaelis-Menten degradation of $StAR$ mRNA. Thus, the function $h_{StAR}(StAR)$ takes the form:

$$h_{StAR}(StAR) = \frac{StAR}{K_{StAR} + StAR} \tag{17}$$

Finally, for the StAR protein dynamics we will account for the 37 kDa precursor, as it has been shown to be the one responsible for cholesterol import before being itself cleaved and imported to the mitochondria [Arakane et al., 1998; Bose et al., 2002; Manna et al., 2009]. It's dynamics is given by:

$$\dot{StARp37} = k_{StARp37} StAR_{\tau_{StARp37}} - \mu_{StARp37} StARp37 \, g^-_{StARp37}(ACTH) \tag{18}$$

where $k_{StARp37}$ stands for the protein translation rate, $\tau_{StARp37}$ is the delay associated to translation, and $\mu_{StARp37} = \gamma_{StARp37} + \epsilon_{StARp37}$ is the $StARp37$ turnover rate. This value accounts for the proteasome-mediated degradation rate of the active precursor $StARp37$, $\gamma_{StARp37}$, and the import rate of the $StARp37$ cleaved byproducts into mitochondria, $\epsilon_{StARp37}$ [Arakane et al., 1997; Bose et al., 2002; Manna et al., 2009]. As it has been show that $StARp37$ activity is proportional to its residence time in the cytosol [Bose et al., 2002; Granot et al., 2003], and that PKA-mediated phosphorylation stabilises the precursor [Clark and Hudson, 2015], we have included the function $g^-_{StARp37}(ACTH)$ in the turnover term in Eq. 18, which takes the form:

$$g^-_{StARp37}(ACTH) = \frac{K^{ACTH}_{StARp37}{}^4}{K^{ACTH}_{StARp37}{}^4 + ACTH^4} \tag{19}$$

1.4 A-CORT Dynamics

As mentioned before, the CORT biosynthetic pathway within the mitochondria won't be modelled explicitly at this stage. Instead, we assume that $ACORT$ dynamics is governed by:

$$\dot{ACORT} = k_{ACORT} f_{ACORT}(StARp37) - \mu_{ACORT} ACORT \tag{20}$$

where k_{ACORT} is the maximum synthesis rate of ACORT, and the turnover term $\mu_{ACORT} = \gamma_{ACORT} + \epsilon_{ACORT}$ accounts for the ACORT degradation rate γ_{ACORT} and the export rate from the adrenal cell into the bloodstream ϵ_{ACORT}. The function f_{ACORT} expresses the dependence of ACORT synthesis on the precursor $StARp37$ and takes the form:

$$f_{ACORT}(StARp37) = \frac{StARp37}{K_{StARp37} + StARp37} \tag{21}$$

where the big K has the same meaning as in previous functions and was determined by fitting the model to data. As mentioned before, $StARp37$ controls the import of cholesterol into the mitochondria [Bose et al., 2002], which is the rate limiting step for corticosteroid biosynthesis. We assumed this process can be represented as a Michaelis-Menten reaction (see Eq. 21) [Arakane et al., 1997; Manna et al., 2009; Spiga et al., 2014]. Importantly, although $StARp37$ is downstream of ACTH (through regulation of the StAR gene), ACORT is known to respond to ACTH stimulation on a much shorter timescale than the time needed for ACTH to exert its effects on $StARp37$ through the cAMP/PKA/pCREB pathway. This likely happens due to PKA mediated $StARp37$ stabilisation in the cytosol upon ACTH stimulation [Arakane et al., 1997; Manna et al., 2009], a process that is already accounted for in the turnover term in Eq. 18.

1.5 pGR Dynamics

Lastly, instead of modelling the concentration of the glucocorticoid receptor, we model the measured levels of its phosphorylated form pGR, a marker of its activity. We propose the dynamics of the pGR is governed by:

$$\dot{pGR} = k_{GR}f_{pGR}(ACORT) - \gamma_{pGR}pGR \tag{22}$$

where k_{pGR} stands for the pGR activation rate by ACORT and γ_{pGR} is it's deactivation rate. The function f_{pGR} takes the form:

$$f_{pGR}(ACORT) = \frac{ACORT}{K_{ACORT} + ACORT} \tag{23}$$

where K_{ACORT} stands for the half-maximum constant of pGR activation by ACORT.

1.6 Model Equations for the SRN

The complete set of model equations is shown below:

$$\dot{dax1} = \sigma_{dax1} + k_{dax1}f_{dax1}(SF1, pGR)g^{-}_{dax1}(ACTH) - \gamma_{dax1}dax1,$$
$$\dot{Dax1} = k_{Dax1}dax1_{\tau_{Dax1}} - \gamma_{Dax1}Dax1g^{\mp}_{Dax1}(ACTH),$$
$$\dot{DAX1} = k_{DAX1}Dax1_{\tau_{DAX1}} - \gamma_{DAX1}DAX1,$$
$$\dot{sf1} = \sigma_{sf1} + k_{sf1}g^{+}_{sf1}(ACTH) - \gamma_{sf1}sf1,$$
$$\dot{Sf1} = k_{Sf1}sf1_{\tau_{Sf1}} - \gamma_{Sf1}h_{Sf1}(Sf1),$$
$$\dot{SF1} = k_{SF1}Sf1_{\tau_{SF1}} - \gamma_{SF1}SF1g^{-}_{SF1}(ACTH),$$
$$\dot{stAR} = \sigma_{stAR} + k_{stAR}f_{stAR}(SF1, DAX1)g^{+}_{stAR}(ACTH) - \gamma_{stAR}stAR,$$
$$\dot{StAR} = k_{StAR}stAR_{\tau_{StAR}} - \gamma_{StAR}h_{StAR}(StAR),$$
$$\dot{StARp37} = k_{StARp37}StAR_{\tau_{StARp37}} - \mu_{StARp37}StARp37g^{-}_{StARp37}(ACTH),$$
$$\dot{ACORT} = k_{ACORT}f_{ACORT}(StARp37) - \mu_{ACORT}ACORT,$$
$$\dot{pGR} = k_{GR}f_{pGR}(ACORT) - \gamma_{pGR}pGR.$$

where:

$$g^{-}_{dax1}(ACTH) = \frac{K^{ACTH^4}_{dax1}}{K^{ACTH^4}_{dax1} + ACTH^4},$$

$$g^{\mp}_{Dax1}(ACTH) = \frac{K^{ACTH-lo}_{Dax1}}{K^{ACTH-lo}_{Dax1} + ACTH} + \frac{ACTH}{K^{ACTH-hi}_{Dax1} + ACTH},$$

$$g^{+}_{sf1}(ACTH) = \frac{ACTH^4}{K^{ACTH^4}_{sf1} + ACTH^4}, \qquad g^{-}_{SF1}(ACTH) = \frac{K^{ACTH}_{SF1}}{K^{ACTH}_{SF1} + ACTH},$$

$$g^{+}_{stAR}(ACTH) = \frac{ACTH^4}{K^{ACTH^4}_{stAR} + ACTH^4}, \qquad g^{-}_{StARp37}(ACTH) = \frac{K^{ACTH}_{StARp37}{}^4}{K^{ACTH}_{StARp37}{}^4 + ACTH^4},$$

$$h_{Sf1}(Sf1) = \frac{Sf1}{K_{Sf1} + Sf1}, \qquad h_{StAR}(StAR) = \frac{StAR}{K_{StAR} + StAR},$$

$$f_{ACORT}(StARp37) = \frac{StARp37}{K_{StARp37} + StARp37}, \qquad f_{pGR}(ACORT) = \frac{ACORT}{K_{ACORT} + ACORT},$$

$$f_{dax1}(SF1, pGR) = \frac{\frac{SF1}{K_{SF1}} + \frac{SF1 \cdot pGR}{K_{SF1} \cdot K_G}}{1 + \frac{SF1}{K_{SF1}} + \frac{SF1 \cdot pGR}{K_{SF1} \cdot K_G}}, \qquad f_{stAR}(SF1, DAX1) = \frac{\frac{SF1}{K_{SF1}}}{1 + \frac{SF1}{K_{SF1}} + \frac{DAX1}{K_D}}.$$

Node	Target	Sign	Effect	References
ACTH	$dax1$	$-$	Inhibits SF1-dependent activation	[Gummow et al., 2006]
	$Dax1$	$\mp$	Modulates mRNA stability	[Ragazzon et al., 2006]
	$sf1$	$+$	Promoter activation	[Ragazzon et al., 2006]
	$SF1$	$-$	Protein stabilisation	[Æsøy et al., 2002]
	$stAR$	$+$	pCREB-mediated promoter activation	[Sugawara et al., 1997a]
				[Sugawara et al., 1997b]
				[Zhao et al., 2005]
				[Manna et al., 2009]
	$StARp37$	$+$	PKA-mediated protein stabilisation	[Arakane et al., 1997]
				[Manna et al., 2009]
	HSL	$+$	PKA-mediated activation (S563 and S660)	[Manna et al., 2013]
		$+$	AMPK-mediated activation (S565)	[Watt et al., 2006]
	$mc2r$	$+$	Promoter activation	[Winnay and Hammer, 2006]
	$mrap$	$+$	Promoter activation	[Gorrigan et al., 2011]
ACORT	pGR	$+$	Activation through phosphorylation	- - -
pGR	$dax1$	$+$	SF1-dependent enhancement of Dax1	[Gummow et al., 2006]
$DAX1$	$stAR$	$+/-$	Inhibits SF1-dependent activation	[Sugawara et al., 1997a]
				[Sugawara et al., 1997b]
				[Fan et al., 2004]
			Activation at high doses	[Xu et al., 2009]
	$mc2r$	$+$	Promoter activation	[Xu et al., 2009]
	$nur77$	$-$	Promoter inhibition	[Song et al., 2004]
	$NUR77$	$-$	Protein inhibition	[Song et al., 2004]
$SF1$	$dax1$	$+$	Promoter activation	[Gummow et al., 2006]
	$stAR/mc2r$	$+$	Promoter activation	[Babu et al., 2002]
				[Gummow et al., 2006]
				[Winnay and Hammer, 2006]
$StARp37$	$StARp30$/Chol	$+$	Cholesterol import to mitochondria	[Arakane et al., 1997]
				[Manna et al., 2009]
	HSL-S660/Chol	$+$	Cholesterol biosynthesis	[Shen et al., 2003]
HSL	S565/S563/S660	$+/-$	Context-dependent phosphorylation	[Kraemer and Shen, 2002]
				[Watt et al., 2006]

Note: Obvious connections (e.g. transcription, translation, ACORT biosynthesis) are not included in this table.

Table A: *Supporting references for cross-talk connections within the adrenal SRN.*

2 Parameter Estimation

The temporal resolution of our experiments is determined by the timescale of the regulatory processes involved, which was in the order of minutes. We set this as the timescale for our kinetic parameters, so that all parametric units were expressed in terms of molar concentrations (M) and minutes (min). Moreover, even though our model equations are considering a single cell system, we must not forget that our experimental measurements were carried out at the tissue level. This means our model predictions could be extrapolated to the total number of cells in the adrenal cortex, provided that the appropriate cellular and nuclear volumes for the different adrenal cell types are accounted for. Though we couldn't find measurements of these volumes in Sprague Dawley rats, we approximated them from a study of the ultrastructure of Wistar rat adrenal cells, which estimates the cell and nuclear volume of steroidogenic ZF cells as $\sim 3600\,\mu m^3$ and $\sim 260\,\mu m^3$, respectively [Nickerson, 1976]. Thus, to deal with Molar units in a simpler way, we used the nuclear volume $V_{nuc} = 2.6 \times 10^{-13}\,lt$ as it is in this cellular enclosure where gene regulatory reactions take place.

Also, note that the regulatory functions have either sigmoidal or Michaelian shapes and that they're normalised (including the multivariate functions). Hence, the overall flux contribution of these terms is to modulate the weight of kinetic rates (small k's), whereas their sensitivity to activation by the independent variable is represented by the half-maximum constants (big K's), i.e. the concentration at which the i-th factor reaches $\frac{1}{2}$.

In what follows, we estimate the kinetic rates and other parameter values. A comprehensive summary of these values is shown in Table B.

2.1 Basal Transcription Rates

The basal transcription rates, denoted by the σ's, are the rates at which the gene promoters are activated without the influence of any of the above-mentioned transcription regulators (thought other factors may be involved), or the minimum level of transcription that these regulators may exert on the gene (see for instance the influx term in Eq. 7 when ACTH is absent). For the sake of simplicity, we assumed that basal transcription rates amounted to 5% of the maximum transcription rates. That is:

$$\sigma_{dax1} = 0.05 * k_{dax1}, \quad \sigma_{sf1} = 0.05 * k_{sf1}, \quad \sigma_{stAR} = 0.05 * k_{stAR}.$$

2.2 Transcription, Translation and Activation Rates

We calculated the maximum rate of gene expression, assessed by the synthesis of the nascent transcript, as:

$$k_{gene} = \frac{k_{pol}^{max}}{L_{hnRNA} N_A V_{nuc}} D_{gene} \tag{24}$$

where k_{gene} is the maximum transcription rate of the gene, measured in Molar concentration per minute; k_{pol}^{max} is the maximum elongation speed (processivity rate) of the RNA polymerase, measured in number of bases synthesised per gene copy per cell per minute and neglecting pauses in polymerase activity; L_{hnRNA} is the hnRNA transcript length, measured in number of bases per transcript (including introns); N_A is Avogadro's constant; V_{nuc} is the nuclear volume of a Zona Fasciculata (ZF) cell, measured in litres; and D_{gene} is the gene dosage, or number of gene copies within each ZF cell.

The maximum processivity rate of the RNA Pol II in mammalian tissue culture cells is estimated at $71.6\,nt/sec$ [Darzacq et al., 2007], corresponding to a maximum elongation speed of $k_{pol}^{max} \approx 4.3\,kb\,min^{-1}$. Regarding the gene dosage, we only have information for human Dax1 present as a duplicate, with both copies active. Thus, we will assume for all genes that $D_{gene} = 2$. The only parameter that remains undetermined in Eq. 24 is the transcript length, which depends on the gene in question and we calculate below.

For the Dax1 gene, which in rats is known to encode a hnRNA of $4129\,b$ in length [3], we estimate a maximum transcription rate of $k_{dax1} = 1.33 \times 10^{-11}\,M\,min^{-1}$ (after splicing, the mature mRNA is reduced to $1.8\,kb$ in length [4]). Similarly, the SF1 gene in rats is known to encode a hnRNA of $20825\,b$ in length [5], which we estimate will have a maximum transcription rate of $k_{sf1} = 2.64 \times 10^{-12}\,M\,min^{-1}$ (after splicing, the mature mRNA is barely $2182\,b$ in length [6]). Lastly, the StAR gene is known to encode a hnRNA of $4643\,b$ in length [7], for which we estimate a maximum transcription rate of $k_{stAR} = 1.18 \times 10^{-11}\,M\,min^{-1}$ (after splicing, the predominant transcript variant is a $3.5\,kb$ mRNA [Ariyoshi et al., 1998]). Thus:

$$k_{dax1} = 1.33 \times 10^{-11}\,M\,min^{-1}, \quad k_{sf1} = 2.64 \times 10^{-12}\,M\,min^{-1}, \quad k_{stAR} = 1.18 \times 10^{-11}\,M\,min^{-1}.$$

which then implies the basal transcription rates are:

$$\sigma_{dax1} = 6.65 \times 10^{-13}\,M\,min^{-1}, \quad \sigma_{sf1} = 1.32 \times 10^{-13}\,M\,min^{-1}, \quad \sigma_{stAR} = 5.91 \times 10^{-13}\,M\,min^{-1}.$$

The maturation rates of hnRNA into mRNA are likely subject to high variability given the post-processing of transcripts depends on multiple, complex reaction steps (e.g. capping, polyadenylation, splicing, nuclear export) [Keene, 2007]. For the sake of simplicity, we'll assume their values are half the above maximum rates of gene expression. Thus, after halving their values and removing Molar units by multiplying by the product of Avogadro's constant and the nuclear volume, we arrive to:

$$k_{Dax1} = 1.04\,min^{-1}, \quad k_{Sf1} = 0.21\,min^{-1}, \quad k_{StAR} = 0.93\,min^{-1}.$$

We calculate the translation rate (protein synthesis) for any given transcript in a single ZF cell as:

$$k_{protein} = \frac{k_{rib}}{L_{poly}} \tag{25}$$

where $k_{protein}$ is the translation rate of the protein per minute per cell (keeping in mind this rate should be multiplied by the Molar concentration of mRNAs, so that protein concentration changes in units of $M\,min^{-1}$); k_{rib} is the polypeptide elongation speed (processivity rate) of the ribosome, measured in number of codons translated (or aa's synthesised) per transcript per cell per minute and assuming ribosome stalling is already accounted for; and L_{poly} is the polypeptide length, measured in number of aa's (we account for the polypeptide length instead of the mRNA length as UTR regions do not contribute to protein synthesis). We will use the average ribosome progression rate for translation in *Mus musculus* as a proxy for that of rat, which was unavailable. This is estimated at 5.6 ± 0.5 codons per second, which equals to $k_{rib} \approx 336\,aa\,min^{-1}$ [Ingolia et al., 2011].

Considering the rat $DAX1$ polypeptide is $472\,aa$ in length [8], we estimate a translation rate of $k_{DAX1} = 0.71\,min^{-1}$. Similarly, the SF1 polypeptide in rats is $462\,aa$ in length [9], which corresponds to a translation rate of $k_{SF1} = 0.73\,min^{-1}$. Lastly, for the StAR protein precursor (the $37\,kDa$ form $StARp37$), we can assume as a "rule of thumb" a molecular weight of 100-110 Da per average amino acid [Phillips et al., 2009]; assuming the newly synthesised $StARp37$ is $\sim 336\,aa$ in length (the 32 kDa form is $284\,aa$ long [10]), we can estimate a translation rate of $k_{StARp37} = 1\,min^{-1}$. Thus:

$$k_{DAX1} = 0.71\,min^{-1}, \quad k_{SF1} = 0.73\,min^{-1}, \quad k_{StARp37} = 1\,min^{-1}.$$

---

[3]http://www.ensembl.org/Rattus_norvegicus/Transcript/Exons?db=core;g=ENSRNOG00000003765;r=X:54734385-54738513;t=ENSRNOT00000005023

[4]http://www.ncbi.nlm.nih.gov/nuccore/NM_053317.1

[5]http://www.ensembl.org/Rattus_norvegicus/Transcript/Exons?db=core;g=ENSRNOG00000012682;r=3:22999616-23020441;t=ENSRNOT00000017651

[6]http://www.ncbi.nlm.nih.gov/nuccore/NM_001191099.1

[7]http://www.ensembl.org/Rattus_norvegicus/Transcript/Exons?db=core;g=ENSRNOG00000015052;r=16:71036204-71040847;t=ENSRNOT00000020606

[8]http://www.uniprot.org/uniprot/P70503

[9]http://www.uniprot.org/uniprot/P50569

[10]http://www.uniprot.org/uniprot/P97826

Lastly, we chose the parameters k_{ACORT} and k_{GR} arbitrarily and allow them to vary during our model fitting to data as a means to probe the negative feedback strength. For these values, we assumed

$$k_{ACORT} = 6.39 \times 10^{-12}\, M\, min^{-1}, \quad k_{GR} = 1 \times 10^{-12}\, M\, min^{-1}.$$

where the chosen value for k_{ACORT} is just 1 divided by the product of the nuclear volume and Avogadro's constant.

2.3 Delays

From the HPA model proposed in [Walker et al., 2010], the overall delay for ACTH signal transduction within the adrenal has been estimated to be $\tau_{Adrenal} \in [6.5, 20]\, min$. However, recent detailed experiments suggest two different time scales for the intra-adrenal network responsiveness, one for the slow genomic pathway and another for the fast, non-genomic one. Specifically, an *intra venous* (i.v.) pulse of ACTH produced rapid, transient increases in plasma CORT, with maximal responses achieved after 5 to 15 min (though some *in vitro* studies show ACTH can trigger CORT synthesis within $\sim 3\, min$), and a decrease to almost basal levels at $\sim 30\, min$. In contrast, $StAR$ and P450scc hnRNA levels increased at 15 min following ACTH and decreased towards basal values after 30 min [Spiga et al., 2011a]. Hence, we can assume $\tau_{Adrenal}^{Non-genomic} \leq 5\, min$ and $\tau_{Adrenal}^{Genomic} \approx 15\, min$.

The case of the StAR gene is of particular interest since it is known to control the limiting step in CORT biosynthesis, which occurs very rapidly during the adrenal response to ACTH stimulation. From [Miller, 2013], we know that on a $15 - 60\, min$ time scale, ACTH rapidly stimulates both the activation of pre-existing StAR protein and its *de novo* the synthesis. ACTH/cAMP doubles the activity of StAR proteins almost immediately [Arakane et al., 1997] and induces transcription of the StAR gene within minutes [Manna et al., 2009]. $StARp37$ then interacts with a complex macromolecular machine in the Outer Mitochondrial Membrane (OMM) that increases the flow of cholesterol from the OMM to the Inner Mitochondrial Membrane (IMM), where it becomes the substrate for CORT biosynthetic enzymes. Thus, we can assume that CORT synthesis is triggered almost instantaneously, whereas StAR gene expression kicks in until a few minutes later.

We can estimate the delays in the genomic pathway by taking into account the gene and hnRNA lengths, together with the processivity rate of the RNA Pol II and the ribosome. The StAR gene, for instance, is known to encode a hnRNA which is $4643\, b$ long. As mentioned before, the maximum processivity rate of the RNA Pol II in mammalian tissue culture cells is estimated at $71.6\, nt/sec = 4.3\, kb/min$ [Darzacq et al., 2007], which means the $StAR$ hnRNA would take $\sim 1.08\, min$ to be transcribed. This transcriptional delay would be unusually short, and we should note that additional processes occur during transcript elongation, such as cumulative pauses of $\sim 4\, min$ in average for polymerases on genes. After accounting for stalling effects on a variety of genes, the same study reports an average processivity rate for RNA Pol II as small as $6.3\, nt/sec$. However, we must keep in mind that these measurements are subject to high variability, depending on the gene, the physiological conditions, and the cell type. For instance, in rat kidney cells the reactivation of serum responsive genes following serum deprivation suggests a synthetic rate of 1.1–$1.4\, kb/min$ [Femino et al., 1998], whereas a more recent study performed on mouse ES cells determined that the RNA Pol II elongation rates ranged between 0.5 to $4\, kb/min$ [Jonkers et al., 2014]. In summary, several studies where measurements were taken by different techniques and in different conditions place the RNA Pol II elongation speed between 18 and $72\, nt/sec$ [Swinburne and Silver, 2008], with most studies reporting values in the lower half of this range. Here, we will assume an average value of $30\, nt/sec = 1.8\, kb/min$.

Using this average processivity rate, the $stAR$ transcriptional delay would be of $2.58\, min$. Regarding transcript editing, we find the duration of an average splicing event has been estimated to last $\sim 30\, sec$ [Hnilicová and Staněk, 2011]. Considering the NCBI reports the StAR gene in *Rattus norvegicus* has 6 introns [11], we can estimate it takes $\sim 3\, min$ for $stAR$ hnRNA to mature into $StAR$ mRNA, assuming introns are removed sequentially instead of simultaneously and neglecting transcript export to the translation site. Regarding translation, a ribosome progression rate of 5.6 ± 0.5

---

[11] http://www.ncbi.nlm.nih.gov/gene/25557

codons per second in *Mus musculus* has been reported [Ingolia et al., 2011]. Considering a newly synthesised $StARp37$ precursor protein would have $\sim 336\,aa$ in length (the 32 kDa form is $284\,aa$ long [12]), we can estimate a translation delay of $\sim 1\,min$ assuming a "rule of thumb" of 100-110 Da per average amino acid [Phillips et al., 2009]. Following this, we estimated the delays for StAR gene expression as

$$\tau_{StAR} = 5.58\,min, \quad \tau_{StARp37} = 1\,min.$$

Likewise, the SF1 gene in rats is known to encode a hnRNA which is $20825\,b$ long. Using the same average RNA Pol II processivity rate as before, we estimate it would take $\sim 11.57\,min$ to be transcribed. As the transcript has 6 introns in total [13], we can estimate $\sim 3\,min$ for hnRNA to mature into mRNA, assuming introns are spliced sequentially and not simultaneously. Regarding translation, and considering the rat $SF1$ polypeptide is $462\,aa$ in length [14], we can estimate a translation delay of $\sim 1.38\,min$. Following this, we estimated the delays for the SF1 gene expression as

$$\tau_{Sf1} = 14.57\,min, \quad \tau_{SF1} = 1.38\,min.$$

Lastly, the Dax1 gene in rats is known to encode a hnRNA which is $4129\,b$ long. Using the same average RNA Pol II processivity rate as before, we estimate it would take $\sim 2.29\,min$ to be transcribed. As the transcript has only 1 intron in total [15], we can estimate $\sim 0.5\,min$ for $dax1$ hnRNA to mature into $Dax1$ mRNA. Regarding translation, and considering the rat $DAX1$ polypeptide is $472\,aa$ in length [16], we can estimate a translation delay of $\sim 1.4\,min$. Following this, we estimated the delays for Dax1 gene expression as

$$\tau_{Dax1} = 2.79\,min, \quad \tau_{DAX1} = 1.4\,min.$$

2.4   Degradation Rates

For simplicity, we'll assume that immature, uncapped, non-polyadenylated hnRNAs will have a degradation rate an order of magnitude faster than their mature mRNA counterparts. This results in half-lives for hnRNAs of $\sim 20\,min$, comparable to those estimated previously for primary transcripts in a model of RNA metabolism in mammalian cells [Jackson et al., 2000]. However, after comparing the model predictions with our data, we required to slightly adjust some of our estimations. This likely arises from previously unaccounted context-dependent degradation processes, as we will see in what follows.

$Dax1$ mRNA half-life is reported by [Ragazzon et al., 2006] to be $3\,hrs$. This value corresponds to a degradation rate of $\gamma_{Dax1} = 3.85 \times 10^{-3}\,min^{-1}$. After fitting the model to data regarding the hnRNA half-life and considering a protein half-life of $6\,hrs$ [Osman et al., 2002], we arrive to the following estimates for the Dax1 gene:

$$\gamma_{dax1} = 1.5 \times 10^{-2}\,min^{-1}, \quad \gamma_{Dax1} = 3.85 \times 10^{-3}\,min^{-1}, \quad \gamma_{DAX1} = 1.93 \times 10^{-3}\,min^{-1}.$$

To the best of our knowledge, there is no data available regarding $Sf1$ mRNA stability. Nonetheless, we can assume that, because its mRNA is ~ 400 bases longer than the $Dax1$ transcript, it degrades at a slower rate. Thus, after calculating a longer half-life in proportion to its length as compared to the $Dax1$ transcript, we estimated a degradation rate for the $Sf1$ mRNA of $3.18 \times 10^{-3}\,min^{-1}$. This rate, however, had to be expressed in different units after the model fitting to data suggested that this degradation was better represented through a Michaelis-Menten mechanism. Thus, the $Sf1$ degradation rate was set to $\gamma_{Sf1} = 2.03 \times 10^{-14}\,M\,min^{-1}$. The $sf1$ hnRNA degradation rate, in contrast, was assumed an order of magnitude larger than its mRNA counterpart. In the proper units, this was set as $\gamma_{sf1} = 3.18 \times 10^{-2}\,min^{-1}$. Regarding the $SF1$ protein, previously [Jacob et al., 2001] and [Chen et al., 2007] have estimated its half-life between $2.5 - 4\,hrs$, corresponding to

---

[12] http://www.uniprot.org/uniprot/P97826
[13] http://www.ncbi.nlm.nih.gov/gene/83826
[14] http://www.uniprot.org/uniprot/P50569
[15] http://www.ncbi.nlm.nih.gov/gene/58850
[16] http://www.uniprot.org/uniprot/P70503

a degradation rate within the range $2.89 \times 10^{-3}\,min^{-1}$ to $4.62 \times 10^{-3}\,min^{-1}$. However, we must take into account the PKA-mediated stabilisation effects of ACTH upon $SF1$. For instance, [Æsøy et al., 2002] found a significant reduction in $SF1$ protein amount in transfected COS-1 cells in the absence of PKA-Cα overexpression measured $4\,hrs$ post chase ($mean \pm SEM = 23.7 \pm 4.64\%$, $P = 0.0022$), compared with the amount of $SF1$ protein after $1\,hr$, which was set to 100%. In contrast, no significant reduction in $SF1$ protein amount was observed after $4\,hrs$ in cells cotransfected with PKA-Cα ($mean \pm SEM = 77.2 \pm 9.5\%$, $P = 0.143$). Thus, it seems that the turnover of transiently expressed $SF1$ was decreased by coexpression of PKA-Cα. Solving the differential equation for first order degradation, we find the degradation rate is given by:

$$\gamma = \frac{1}{t} \ln \frac{x_0}{x(t)} \tag{26}$$

which we can use to calculate $\gamma_{SF1}^{PKA-} = 8 \times 10^{-3}\,min^{-1}$ and $\gamma_{SF1}^{PKA+} = 1.44 \times 10^{-3}\,min^{-1}$. Here, we will use the first value, as by including the function $g_{SF1}^{-}(ACTH)$ in the turnover term in Eq. 11 we account for the PKA-mediated stabilising effects of ACTH stimuli. Thus, for the SF1 gene, in the absence of ACTH stimulation, we will have:

$$\gamma_{sf1} = 3.18 \times 10^{-2}\,min^{-1}, \quad \gamma_{Sf1} = 2.03 \times 10^{-14}\,M\,min^{-1}, \quad \gamma_{SF1} = 8 \times 10^{-3}\,min^{-1}.$$

The available information regarding $StAR$ mRNA stability is a bit controversial, especially since two isoforms have been reported, each with different half-lives and the possibility of selective degradation in steroidogenic cells [Duan and Jefcoate, 2007]. As before, we could make an estimation based on its transcript length being twice as long as the $Dax1$ mRNA. Following this, we estimated a degradation rate of $1.98 \times 10^{-3}\,min^{-1}$. However, at the moment of fitting the model to data from the ACTH i.v. pulse experiment, we found that this degradation rate had to be approximately twice as large. Accordingly, we have modified it to $\gamma_{StAR} = 3.96 \times 10^{-3}\,min^{-1}$. Likewise, the value of the $stAR$ hnRNA degradation was adjusted after fitting the model to data and was fixed at $\gamma_{stAR} = 1 \times 10^{-1}\,min^{-1}$. The increase in the γ_{StAR} degradation rate, when compared to the value we originally estimated for $StAR$ mRNA is also supported by experimental evidence showing this gene contains three conserved AU-rich (AURE) element motifs known to mediate fast mRNA turnover [Zhao et al., 2005; Duan and Jefcoate, 2007]. Moreover, the measured half-life for the $3.5\,kb$ $StAR$ mRNA isoform corresponds to a degradation rate of $3.3 \times 10^{-3}\,min^{-1}$, which is close to our estimated value.

The estimation of the $StARp37$ protein turnover rate requires careful examination. According to [Arakane et al., 1997], the StAR protein has a short half-life, but a specific value is not reported. The half-life reported by [Ragazzon et al., 2006] is $\sim 5\,hrs$, with the primary source being [Granot et al., 2003]. However, this value refers to mitochondrial $30\,kDa\,StAR$, which lacks the N-terminus mitochondrial targeting sequence and it's not involved in cholesterol import into mitochondria. This sequence is cleaved upon the $StAR\,37\,kDa$ import into mitochondria, a process that influences the rate of the $StARp37$ precursor cytosolic proteasome degradation, according to [Granot et al., 2003].

Both [Arakane et al., 1998] and [Granot et al., 2003] estimate that the $StARp37$ precursor has a half-life of $\sim 15\,min$. However, this estimate accounts only for proteasome-assisted degradation, and the authors suggest that a fast import of the precursor into mitochondria would decrease the time it remains active. This would effectively increase the precursor's lability when both degradation and translocation processes are accounted for, thus decreasing the half-life to $\leq 5\,min$ [Manna et al., 2009; Clark and Hudson, 2015]. This is consistent with previous estimations of $StARp37$ exhibiting a half-life of $5\,min$ in mouse Y1 cells [Artemenko et al., 2001], and of $3 - 4\,min$ in rat adrenal cells incubated at 37 ℃ [Epstein and Orme-Johnson, 1991].

How then is it possible for adrenal cells to exhibit such a fast steroidogenic response while depending upon a precursor protein that is so labile? As it turns out, PKA-mediated ACTH stimulation induces rapid phosphorylation of the precursor $StARp37$, thus stabilising it in the cytosol and enhancing its activity. In other words, ACTH stimulation increases the residence time of $StARp37$ in the cytosol, thus increasing the rate of cholesterol import into mitochondria and enabling the fast response of the adrenal to synthesise CORT.

In summary, we have that when mitochondrial import is blocked, the half-life of the StAR precursor is $15\,min$, corresponding to $\gamma_{StARp37} = 4.62 \times 10^{-2}\,min^{-1}$; but when both mechanisms are blocked the precursor accumulates in the cytosol and its half-life increases up to $6.5\,hrs$, corresponding to a much lower turnover rate of $\mu_{StARp37} = \gamma_{StARp37} + \epsilon_{StARp37} = 1.78 \times 10^{-3}\,min^{-1}$ [Granot et al., 2003]. In contrast, when both protein degradation and mitochondrial import are fully functional, and in the absence of ACTH stimulation, the protein is extremely labile, with a half-life of $\sim 3.5\,min$, corresponding to $\mu_{StARp37}^{ACTH-} = \gamma_{StARp37} + \epsilon_{StARp37} = 1.98 \times 10^{-1}\,min^{-1}$ [Epstein and Orme-Johnson, 1991]. However, upon PKA-mediated phosphorylation of the precursor after ACTH stimulation, the $StARp37$ stabilises and its effective turnover rate drops by two orders of magnitude down to $\mu_{StARp37}^{ACTH+} = \gamma_{StARp37} + \epsilon_{StARp37} = 1.49 \times 10^{-3}\,min^{-1}$ [Clark and Hudson, 2015]. Thus

$$\mu_{StARp37}^{ACTH-} = 1.98 \times 10^{-1}\,min^{-1}$$
$$\mu_{StARp37}^{ACTH+} = 1.49 \times 10^{-3}\,min^{-1}$$

The transition from a very high to a very low turnover rate for $StARp37$ is represented in the second term in Eq. 18 by introducing the function $g_{StARp37}^{-}(ACTH)$ (Eq. 19), which modulates the removal rate $\mu_{StARp37}$. As the decrease in the turnover rate upon ACTH stimulation is quite large, we can fix the parameter as $\mu_{StARp37} = 1.98 \times 10^{-1}\,min^{-1}$ when no ACTH stimulation is present and let the function $g_{StARp37}^{-}(ACTH)$ stabilise $StARp37$. Summarising for the StAR gene, the turnover rates are:

$$\gamma_{stAR} = 1 \times 10^{-1}\,min^{-1}, \quad \gamma_{StAR} = 3.96 \times 10^{-3}\,min^{-1}, \quad \gamma_{StARp37} = 1.98 \times 10^{-1}\,min^{-1}.$$

Though the half-life of intra-adrenal corticosterone ($ACORT$) has not been measured directly, given its rapid export to the bloodstream we can assume it has a faster removal rate than its plasma counterpart. Assuming a half-life of $1\,min$, we estimate a turnover rate of

$$\mu_{ACORT} = 6.93 \times 10^{-1}\,min^{-1}$$

Lastly, for the phosphorylated glucocorticoid receptor (pGR), we find from [Bodwell et al., 1998] that the mouse GR is very stable, with a half-life of $\sim 18\,hrs$ (reduced down to $8-9\,hrs$ upon dexamethasone stimulation). However, we're interested in the half-life of the active, phosphorylated form of GR. This is likely to be much more short-lived, but nonetheless has not been measured. For the sake of simplicity, we assume it's half-life is the same as that of $ACORT$, which implies a turnover rate of

$$\gamma_{pGR} = 6.93 \times 10^{-1}\,min^{-1}$$

2.5 Half-Maximum Constants

The half-maximum constants (big K's) are arbitrary parameters that nonetheless capture the sensitivity of a process (e.g. synthesis or degradation) affecting the dynamics of a molecular species Y as a function of the concentration of another species X. As the molecular mechanisms underlying these processes are often unknown, we model them as Michaelis-Menten and Hill type functions. In the latter case, when the Hill coefficient is high enough, these K's could also be interpreted as activation thresholds. Though arbitrary, their relative values are informative of how sensitive different nodes within the adrenal SRN are to common external *stimuli* (e.g. ACTH and cytokines).

Half-maximum constants were estimated manually after observing the system's time evolution and correcting our model for the timescales at which the peak of the transient response, together with the rising and decreasing phases, followed the experimental data. The estimated K's are listed in Table B and represented graphically in Fig. S9. The half-maximum constants that are neither dependent on ACTH nor cytokines, but are rather involved in $Dax1$, $Sf1$ and $StAR$ mRNA degradation, in $ACORT$ and pGR synthesis, and in regulation of Dax1 and StAR gene promoters, were also fixed manually to values close to the range observed during their circadian dynamics.

Of particular interest are the constants $K_{Dax1}^{ACTH-lo}$ and $K_{Dax1}^{ACTH-hi}$ which, respectively, represent the lower and upper *near* half-maximum constants for a non-monotonous regulatory function (Eq. 5)

that models dose-dependent effects of ACTH upon $Dax1$ mRNA stability (Fig. S4). We hypothesise that this dose-dependent degradation of $Dax1$ mRNA could be a post-transcriptional regulatory mechanism such as stress-induced non-sense mediated mRNA decay [He and Jacobson, 2015].

Basal Transcription Rates		
$\sigma_{dax1} = 6.65 \times 10^{-13}\, M\, min^{-1}$	$\sigma_{sf1} = 1.32 \times 10^{-13}\, M\, min^{-1}$	$\sigma_{stAR} = 5.91 \times 10^{-13}\, M\, min^{-1}$
Transcription, Translation and Activation Rates		
$k_{dax1} = 1.33 \times 10^{-11}\, M\, min^{-1}$	$k_{sf1} = 2.64 \times 10^{-12}\, M\, min^{-1}$	$k_{stAR} = 1.18 \times 10^{-11}\, M\, min^{-1}$
$k_{Dax1} = 1.04\, min^{-1}$	$k_{Sf1} = 0.21\, min^{-1}$	$k_{StAR} = 0.93\, min^{-1}$
$k_{DAX1} = 0.71\, min^{-1}$	$k_{SF1} = 0.73\, min^{-1}$	$k_{StARp37} = 1\, min^{-1}$
$k_{ACORT} = 6.39 \times 10^{-12}\, M\, min^{-1}$	$k_{GR} = 1 \times 10^{-12}\, M\, min^{-1}$	
Degradation Rates		
$\gamma_{dax1} = 1.5 \times 10^{-2}\, min^{-1}$	$\gamma_{sf1} = 3.18 \times 10^{-2}\, min^{-1}$	$\gamma_{stAR} = 1 \times 10^{-1}\, min^{-1}$
$\gamma_{Dax1} = 3.85 \times 10^{-3}\, min^{-1}$	$\gamma_{Sf1} = 2.03 \times 10^{-14}\, M\, min^{-1}$	$\gamma_{StAR} = 3.96 \times 10^{-3}\, min^{-1}$
$\gamma_{DAX1} = 1.93 \times 10^{-3}\, min^{-1}$	$\gamma_{SF1} = 8 \times 10^{-3}\, min^{-1}$	$\mu_{StARp37} = 1.98 \times 10^{-1}\, min^{-1}$
$\mu_{ACORT} = 6.93 \times 10^{-1}\, min^{-1}$	$\gamma_{pGR} = 6.93 \times 10^{-1}\, min^{-1}$	
Delays		
$\tau_{Dax1} = 2.79\, min$	$\tau_{Sf1} = 14.57\, min$	$\tau_{StAR} = 5.58\, min$
$\tau_{DAX1} = 1.4\, min$	$\tau_{SF1} = 1.38\, min$	$\tau_{StARp37} = 1\, min$
Half-Maximum Constants		
$K_{dax1}^{ACTH} = 90\, pg\, ml^{-1}$	$K_{ACORT} = 4.5\, AU$	$K_{dax1}^{IL6} = K_{Dax1}^{IL6} = K_{DAX1}^{IL6} = 500\, AU$
$K_{Dax1}^{ACTH-lo} = 30\, pg\, ml^{-1}$	$K_{G} = 0.76\, AU$	$K_{sf1}^{IL6} = 1000\, AU$
$K_{Dax1}^{ACTH-hi} = 1000\, pg\, ml^{-1}$	$K_{D} = 5.7 \times 10^{-5}\, M$	$K_{Sf1}^{IL6} = K_{SF1}^{IL6} = 100\, AU$
$K_{sf1}^{ACTH} = 30\, pg\, ml^{-1}$	$K_{Sf1} = 1 \times 10^{-8}\, M$	$K_{StAR}^{IL6} = 2500\, AU$
$K_{SF1}^{ACTH} = 70\, pg\, ml^{-1}$	$K_{SF1} = 6.2 \times 10^{-7}\, M$	$K_{StARp37}^{IL6} = 500\, AU$
$K_{stAR}^{ACTH} = 70\, pg\, ml^{-1}$	$K_{StAR} = 1 \times 10^{-8}\, M$	$K_{stAR}^{IL1\beta} = 200\, AU$
$K_{StARp37}^{ACTH} = 70\, pg\, ml^{-1}$	$K_{StARp37} = 4 \times 10^{-8}\, M$	$K_{stAR}^{TNF\alpha} = K_{StAR}^{TNF\alpha} = 60\, AU$
		$K_{pGR}^{TNF\alpha} = 20\, AU$

Table B: *Kinetic rates and other estimated parameter values.*

3 Crosstalk Between the Adrenal SRN and the Immune Pathway

Stimulation of rats with the bacterial lipopolysaccharide (LPS) endotoxin elicits a strong response not only at the HPA level but also on the immune system. In particular, LPS induces cytokines $TNF\alpha$, $IL1\beta$ and $IL6$[17], which are known to act upon targets of the adrenal SRN and among themselves.

A previous mathematical model by [Malek et al., 2015] suggested a way in which LPS, $TNF\alpha$ and $IL6$ may interact with ACTH and CORT to mediate the adrenal response to inflammation. However, such a model assumed direct interactions of these cytokines upon ACTH, ignoring the steroidogenic pathway within adrenal cells. LPS effects on the immune system are more complex and start with the recruitment of macrophages to the adrenal cortex. This increases levels of $TNF\alpha$ in a first stage (peak at $60\,min$), and of $IL1\beta$ and $IL6$ (in T-lymphocytes) in a second stage (peaks at $120\,min$) [Givalois et al., 1994]. While it is believed that the first stage is amplified through a positive feedback, in the second one $IL1\beta$ and $IL6$ are known to inhibit rising levels of $TNF\alpha$. Moreover, though CORT is known to inhibit both $IL1\beta$ and $IL6$, it has been proposed that $IL1\beta$ is involved in the initial activation of CORT production, whereas $IL6$ sustains it [Givalois et al., 1994; Kanczkowski et al., 2013]. These interactions between LPS and cytokines, together with the crosstalk between the immune pathway and the adrenal SRN (Table C), is summarised in Fig. S8.

Even though the interactions among cytokines are complex, we know that the output of the internal crosstalk within the immune pathway upon an LPS challenge delivers the measured levels of $TNF\alpha$, $IL1\beta$ and $IL6$ (Fig. S7a-c). Thus, we can ignore the interactions within the immune pathway as long as we account for the effects of cytokines upon specific targets of the adrenal SRN. This effectively means that, during an LPS challenge, in addition to an ACTH input we will now use the time course of these cytokines as input functions. The task becomes complex as soon as we realise that the experimental evidence available comes from different cell types and animal models (Table C).

3.1 Model Equations for the SRN with Cytokine Interactions

We explored different network architectures and arrived to the scenario depicted in Fig. 5, which is associated to the following set of model equations, where the cytokine effects are shown in red:

$$\dot{dax1} = \sigma_{dax1} + k_{dax1}f_{dax1}(SF1, pGR)g^-_{dax1}(ACTH)\phi_{dax1}(IL6) - \gamma_{dax1}dax1,$$

$$\dot{Dax1} = k_{Dax1}dax1_{\tau_{Dax1}}\phi_{Dax1}(IL6) - \gamma_{Dax1}Dax1g^\mp_{Dax1}(ACTH),$$

$$\dot{DAX1} = k_{DAX1}Dax1_{\tau_{DAX1}}\phi_{DAX1}(IL6) - \gamma_{DAX1}DAX1,$$

$$\dot{sf1} = \sigma_{sf1} + k_{sf1}g^+_{sf1}(ACTH)\phi_{sf1}(IL6) - \gamma_{sf1}sf1,$$

$$\dot{Sf1} = k_{Sf1}sf1_{\tau_{Sf1}}\phi_{Sf1}(IL6) - \gamma_{Sf1}h_{Sf1}(Sf1),$$

$$\dot{SF1} = k_{SF1}Sf1_{\tau_{SF1}}\phi_{SF1}(IL6) - \gamma_{SF1}SF1g^-_{SF1}(ACTH),$$

$$\dot{stAR} = \sigma_{stAR} + k_{stAR}f_{stAR}(SF1, DAX1)g^+_{stAR}(ACTH)\phi_{stAR}(TNF\alpha)\phi_{stAR}(IL1\beta) - \gamma_{stAR}stAR,$$

$$\dot{StAR} = k_{StAR}stAR_{\tau_{StAR}}\phi_{StAR}(TNF\alpha)\phi_{StAR}(IL6) - \gamma_{StAR}h_{StAR}(StAR),$$

$$\dot{StARp37} = k_{StARp37}StAR_{\tau_{StARp37}}\phi_{StARp37}(IL6) - \mu_{StARp37}StARp37g^-_{StARp37}(ACTH),$$

$$\dot{ACORT} = k_{ACORT}f_{ACORT}(StARp37) - \mu_{ACORT}ACORT,$$

$$\dot{pGR} = k_{GR}f_{pGR}(ACORT)\phi_{pGR}(TNF\alpha) - \gamma_{pGR}pGR.$$

---

[17]The hyphen in *TNF-α*, *IL-1β*, and *IL-6* labels was dropped to avoid confusion with a minus sign.

where

$$\phi_{dax1}(IL6) = \frac{K_{dax1}^{IL6}}{K_{dax1}^{IL6} + IL6}, \qquad \phi_{stAR}(TNF\alpha) = 1 + \frac{TNF\alpha}{K_{stAR}^{TNF\alpha} + TNF\alpha},$$

$$\phi_{Dax1}(IL6) = \frac{K_{Dax1}^{IL6}}{K_{Dax1}^{IL6} + IL6}, \qquad \phi_{stAR}(IL1\beta) = 1 + \frac{IL1\beta}{K_{stAR}^{IL1\beta} + IL1\beta},$$

$$\phi_{DAX1}(IL6) = \frac{K_{DAX1}^{IL6}}{K_{DAX1}^{IL6} + IL6}, \qquad \phi_{StAR}(TNF\alpha) = 1 + \frac{TNF\alpha}{K_{StAR}^{TNF\alpha} + TNF\alpha},$$

$$\phi_{sf1}(IL6) = \frac{K_{sf1}^{IL6^4}}{K_{sf1}^{IL6^4} + IL6^4}, \qquad \phi_{StAR}(IL6) = \frac{K_{StAR}^{IL6}}{K_{StAR}^{IL6} + IL6},$$

$$\phi_{Sf1}(IL6) = \frac{K_{Sf1}^{IL6^4}}{K_{Sf1}^{IL6^4} + IL6^4}, \qquad \phi_{StARp37}(IL6) = \frac{K_{StARp37}^{IL6}}{K_{StARp37}^{IL6} + IL6},$$

$$\phi_{SF1}(IL6) = \frac{K_{SF1}^{IL6}}{K_{SF1}^{IL6} + IL6}, \qquad \phi_{pGR}(TNF\alpha) = \frac{K_{pGR}^{TNF\alpha}}{K_{pGR}^{TNF\alpha} + TNF\alpha}.$$

As before, the half-maximum constants for the cytokine effects upon targets of the adrenal SRN can be understood as sensitivities. These were estimated by manually fitting the model predictions to experimental data from the LPS challenge experiments. The values are listed in Table B and represented graphically in Fig. S9d-f.

Cytokine	Target	Sign	Cell type/species	Reference
$TNF\alpha$	StAR mRNA/protein	−	Rat testis Leydig tumor cells (LC-540)	[Sadasivam et al., 2015]
	StAR mRNA/protein	−	Mouse macrophage cell line (RAW264.7)	[Ma et al., 2007]
	DAX1 protein	+	Rat testis Leydig tumor cells (LC-540)	[Sadasivam et al., 2015]
	StAR mRNA	+	Human adrenocortical cells (NCI-H295R)	[Tkachenko et al., 2011]
	Cortisol	−	Bovine Zone Fasciculata cells	[Barney et al., 2000]
	pGR	−	Human Airway Smooth Muscle cells	[Bouazza et al., 2012]
$IL1\beta$	StAR mRNA	+	Human adrenocortical cells (NCI-H295R)	[Tkachenko et al., 2011]
$IL6$	StAR mRNA/protein	+	Bovine Zona Fasciculata cells	[McIlmoil et al., 2016]
	Dax1 mRNA/protein	−	Bovine Zona Fasciculata cells	[McIlmoil et al., 2016]
	SF1 mRNA/protein	+	Bovine Zona Fasciculata cells	[McIlmoil et al., 2016]
	StAR mRNA/protein	−	Bovine Zona Reticularis cells	[McIlmoil et al., 2015]
	Dax1 mRNA/protein	+	Bovine Zona Reticularis cells	[McIlmoil et al., 2015]
	SF1 mRNA/protein	−	Bovine Zona Reticularis cells	[McIlmoil et al., 2015]
	StAR mRNA	+	Human adrenocortical cells (NCI-H295R)	[Tkachenko et al., 2011]
	Cortisol	+	Bovine Zona Fasciculata cells	[Barney et al., 2000]
LPS	StAR 30 kDa	−	Rat testis Leydig cells	[Allen et al., 2004]
				[Held Hales et al., 2000]
	StAR 30 kDa	+	Rat adrenal cells	[Held Hales et al., 2000]
	StAR 37 kDa	+	Rat testis Leydig tumor cells	[Allen et al., 2004]
	StAR	+	Mouse Y1 cells	[Calejman et al., 2011]
	Corticosterone	+	Rat adrenal cells	[Calejman et al., 2011]

Table C: *Cytokine effects upon targets within the adrenal SRN.*

3.2 Scaling Model Outputs of Cytokine Targets

Even though our model predicts the time evolution of hnRNA, mRNA, and protein concentrations, these predictions are inherently qualitative. This is mainly because we have approximated the mechanisms underlying gene regulation through Hill type functions and, to a lesser degree, because our model doesn't account for regulatory processes affecting mRNA and protein stability.

However, in order to make our model predictions comparable to the experimental data (expressed in $pg/\mu g$ for ACORT and as fold induction for all other variables), we have implemented a variable change to express the model predictions in terms of dimensionless arbitrary units. To do this consistently, all x state variables in the model were transformed according to the formula:

$$\hat{x} = \frac{x - x_{t=0}}{x_{max} - x_{min}} \sigma_x + \textit{offset}$$

where $x_{t=0}$ is the value of x at the time the pulse is given, x_{max} and x_{min} are the maximum and minimum value of the response, and σ_x is a scaling factor. The *offset* value was set to 1 for all state variables with data reported as fold induction, except for ACORT, which experiments reported as $pg/\mu g$ and for which we set an *offset* of 25, following the baseline observed in ACTH i.v. pulse experiments.

The scaling factors were adjusted to reproduce the data of the ACTH i.v. pulse experiment, and these remained invariant when the model was used to predict the high s.c. ACTH pulse and LPS challenge data without cytokines (Table D). The only scenario where scaling factors were allowed to vary was after modifying the existing model to account for cytokine effects. Interestingly, in this latter case most scaling factors remain invariant, except for those multiplying variables targeted by cytokines. As before, this is because we have used Hill type functions to approximate the mechanisms by which these pro-inflammatory cytokines interact with targets of the SRN.

Variable	ACTH small i.v. pulse	ACTH high s.c. pulse	LPS challenge without cytokines	LPS challenge with cytokines
ACORT	300	300	300	300
pGR	3.5	3.5	3.5	0.4
dax1 hnRNA	0.9	0.9	0.9	0.9
Dax1 mRNA	0.4	0.4	0.4	0.8
DAX1 protein	0.1	0.1	0.1	0.6
sf1 hnRNA	0.6	0.6	0.6	0.6
Sf1 mRNA	0.5	0.5	0.5	0.1
SF1 protein	0.2	0.2	0.2	0.2
stAR hnRNA	3	3	3	3
StAR mRNA	2	2	2	2
StARp37 protein	0.1	0.1	0.1	2

Table D: *Scaling factors σ_x. Values in red correspond to non-statistically significant data. All scaling factors remain invariant in the model, except when the model is modified to account for cytokine inputs (last column) and only on molecular species targeted by cytokines (Fig. 5).*

References

Allen, J. A., Diemer, T., Janus, P., Hales, K. H., and Hales, D. B. (2004). Bacterial endotoxin lipopolysaccharide and reactive oxygen species inhibit leydig cell steroidogenesis via perturbation of mitochondria. *Endocrine*, 25(3):265–275.

Arakane, F., Kallen, C. B., Watari, H., Foster, J. A., Sepuri, N. B. V., Pain, D., Stayrook, S. E., Lewis, M., Gerton, G. L., and Strauss, J. F. (1998). The mechanism of action of steroidogenic acute regulatory protein (star) star acts on the outside of mitochondria to stimulate steroidogenesis. *Journal of Biological Chemistry*, 273(26):16339–16345.

Arakane, F., King, S. R., Du, Y., Kallen, C. B., Walsh, L. P., Watari, H., Stocco, D. M., and Strauss, J. F. (1997). Phosphorylation of steroidogenic acute regulatory protein (star) modulates its steroidogenic activity. *Journal of Biological Chemistry*, 272(51):32656–32662.

Ariyoshi, N., Kim, Y.-C., Artemenko, I., Bhattacharyya, K. K., and Jefcoate, C. R. (1998). Characterization of the rat star gene that encodes the predominant 3.5-kilobase pair mrna acth stimulation of adrenal steroids in vivo precedes elevation of star mrna and protein. *Journal of Biological Chemistry*, 273(13):7610–7619.

Artemenko, I. P., Zhao, D., Hales, D. B., Hales, K. H., and Jefcoate, C. R. (2001). Mitochondrial processing of newly synthesized steroidogenic acute regulatory protein (star), but not total star, mediates cholesterol transfer to cytochrome p450 side chain cleavage enzyme in adrenal cells. *Journal of Biological Chemistry*, 276(49):46583–46596.

Babu, P. S., Bavers, D. L., Beuschlein, F., Shah, S., Jeffs, B., Jameson, J. L., and Hammer, G. D. (2002). Interaction between dax-1 and steroidogenic factor-1 in vivo: increased adrenal responsiveness to acth in the absence of dax-1. *Endocrinology*, 143(2):665–673.

Barney, M., Call, G. B., McIlmoil, C. J., Husein, O. F., Adams, A., Balls, A. G., Oliveira, G. K., Miner, E. C., Richards, T. A., Crawford, B. K., et al. (2000). Stimulation by interleukin-6 and inhibition by tumor necrosis factor of cortisol release from bovine adrenal zona fasciculata cells through their receptors. *Endocrine*, 13(3):369–377.

Bodwell, J. E., Webster, J. C., Jewell, C. M., Cidlowski, J. A., Hu, J.-M., and Munck, A. (1998). Glucocorticoid receptor phosphorylation: overview, function and cell cycle-dependence. *The Journal of steroid biochemistry and molecular biology*, 65(1):91–99.

Bose, H. S., Lingappa, V. R., and Miller, W. L. (2002). Rapid regulation of steroidogenesis by mitochondrial protein import. *Nature*, 417(6884):87–91.

Bouazza, B., Krytska, K., Debba-Pavard, M., Amrani, Y., Honkanen, R. E., Tran, J., and Tliba, O. (2012). Cytokines alter glucocorticoid receptor phosphorylation in airway cells: role of phosphatases. *American journal of respiratory cell and molecular biology*, 47(4):464–473.

Calejman, C. M., Astort, F., Di Gruccio, J., Repetto, E., Mercau, M., Giordanino, E., Sanchez, R., Pignataro, O., Arias, P., and Cymeryng, C. (2011). Lipopolysaccharide stimulates adrenal steroidogenesis in rodent cells by a nfκb-dependent mechanism involving cox-2 activation. *Molecular and cellular endocrinology*, 337(1):1–6.

Chen, W.-Y., Weng, J.-H., Huang, C.-C., and Chung, B.-c. (2007). Histone deacetylase inhibitors reduce steroidogenesis through scf-mediated ubiquitination and degradation of steroidogenic factor 1 (nr5a1). *Molecular and cellular biology*, 27(20):7284–7290.

Clark, B. J. and Hudson, E. A. (2015). Star protein stability in y1 and kin-8 mouse adrenocortical cells. *Biology*, 4(1):200–215.

Darzacq, X., Shav-Tal, Y., de Turris, V., Brody, Y., Shenoy, S. M., Phair, R. D., and Singer, R. H. (2007). In vivo dynamics of rna polymerase ii transcription. *Nature structural molecular biology*, 14(9):796–806.

Duan, H. and Jefcoate, C. R. (2007). The predominant camp-stimulated 3.5 kb star mrna contains specific sequence elements in the extended 3 utr that confer high basal instability. *Journal of molecular endocrinology*, 38(1):159–179.

Epstein, L. and Orme-Johnson, N. (1991). Regulation of steroid hormone biosynthesis. identification of precursors of a phosphoprotein targeted to the mitochondrion in stimulated rat adrenal cortex cells. *Journal of Biological Chemistry*, 266(29):19739–19745.

Ermentrout, B. (2002). *Simulating, analyzing, and animating dynamical systems: a guide to XP-PAUT for researchers and students*, volume 14. Siam.

Fan, W., Yanase, T., Wu, Y., Kawate, H., Saitoh, M., Oba, K., Nomura, M., Okabe, T., Goto, K., and Yanagisawa, J. (2004). Protein kinase a potentiates adrenal 4 binding protein/steroidogenic factor 1 transactivation by reintegrating the subcellular dynamic interactions of the nuclear receptor with its cofactors, general control nonderepressed-5/transformation/transcription domain-associated protein, and suppressor, dosage-sensitive sex reversal-1: a laser confocal imaging study in living kgn cells. *Molecular Endocrinology*, 18(1):127–141.

Femino, A. M., Fay, F. S., Fogarty, K., and Singer, R. H. (1998). Visualization of single rna transcripts in situ. *Science*, 280(5363):585–590.

Givalois, L., Dornand, J., Mekaouche, M., Solier, M., Bristow, A., Ixart, G., Siaud, P., Assenmacher, I., and Barbanel, G. (1994). Temporal cascade of plasma level surges in acth, corticosterone, and cytokines in endotoxin-challenged rats. *American Journal of Physiology-Regulatory, Integrative and Comparative Physiology*, 267(1):R164–R170.

Gorrigan, R. J., Guasti, L., King, P., Clark, A. J., and Chan, L. F. (2011). Localisation of the melanocortin-2-receptor and its accessory proteins in the developing and adult adrenal gland. *Journal of molecular endocrinology*, 46(3):227–232.

Granot, Z., Geiss-Friedlander, R., Melamed-Book, N., Eimerl, S., Timberg, R., Weiss, A. M., Hales, K. H., Hales, D. B., Stocco, D. M., and Orly, J. (2003). Proteolysis of normal and mutated steroidogenic acute regulatory proteins in the mitochondria: the fate of unwanted proteins. *Molecular Endocrinology*, 17(12):2461–2476.

Gummow, B. M., Scheys, J. O., Cancelli, V. R., and Hammer, G. D. (2006). Reciprocal regulation of a glucocorticoid receptor-steroidogenic factor-1 transcription complex on the dax-1 promoter by glucocorticoids and adrenocorticotropic hormone in the adrenal cortex. *Mol Endocrinol*, 20(11):2711–23.

He, F. and Jacobson, A. (2015). Nonsense-mediated mrna decay: degradation of defective transcripts is only part of the story. *Annual review of genetics*, 49:339–366.

Held Hales, K., Diemer, T., Ginde, S., Shankar, B. K., Roberts, M., Bosmann, H. B., and Hales, D. B. (2000). Diametric effects of bacterial endotoxin lipopolysaccharide on adrenal and leydig cell steroidogenic acute regulatory protein. *Endocrinology*, 141(11):4000–4012.

Hnilicová, J. and Staněk, D. (2011). Where splicing joins chromatin. *Nucleus*, 2(3):182–188.

Ingolia, N. T., Lareau, L. F., and Weissman, J. S. (2011). Ribosome profiling of mouse embryonic stem cells reveals the complexity and dynamics of mammalian proteomes. *Cell*, 147(4):789–802.

Iyer, A. K., Zhang, Y.-H., and McCabe, E. R. (2007). Lxxll motifs and af-2 domain mediate shp (nr0b2) homodimerization and dax1 (nr0b1)–dax1a heterodimerization. *Molecular genetics and metabolism*, 92(1):151–159.

Jackson, D. A., Pombo, A., and Iborra, F. (2000). The balance sheet for transcription: an analysis of nuclear rna metabolism in mammalian cells. *The FASEB Journal*, 14(2):242–254.

Jacob, A. L., Lund, J., Martinez, P., and Hedin, L. (2001). Acetylation of steroidogenic factor 1 protein regulates its transcriptional activity and recruits the coactivator gcn5. *Journal of Biological Chemistry*, 276(40):37659–37664.

Jasper, M. and Engeland, W. (1994). Splanchnic neural activity modulates ultradian and circadian rhythms in adrenocortical secretion in awake rats. *Neuroendocrinology*, 59(2):97–109.

Jonkers, I., Kwak, H., and Lis, J. T. (2014). Genome-wide dynamics of pol ii elongation and its interplay with promoter proximal pausing, chromatin, and exons. *Elife*, 3:e02407.

Kanczkowski, W., Chatzigeorgiou, A., Samus, M., Tran, N., Zacharowski, K., Chavakis, T., and Bornstein, S. R. (2013). Characterization of the lps-induced inflammation of the adrenal gland in mice. *Molecular and cellular endocrinology*, 371(1):228–235.

Keene, J. D. (2007). Rna regulons: coordination of post-transcriptional events. *Nature Reviews Genetics*, 8(7):533–543.

Kitay, J. I. (1961). Sex differences in adrenal cortical secretion in the rat 1. *Endocrinology*, 68(5):818–824.

Kraemer, F. B. and Shen, W.-J. (2002). Hormone-sensitive lipase control of intracellular tri-(di-) acylglycerol and cholesteryl ester hydrolysis. *Journal of lipid research*, 43(10):1585–1594.

Ma, Y., Ren, S., Pandak, W., Li, X., Ning, Y., Lu, C., Zhao, F., and Yin, L. (2007). The effects of inflammatory cytokines on steroidogenic acute regulatory protein expression in macrophages. *Inflammation research*, 56(12):495–501.

Malek, H., Ebadzadeh, M. M., Safabakhsh, R., Razavi, A., and Zaringhalam, J. (2015). Dynamics of the hpa axis and inflammatory cytokines: Insights from mathematical modeling. *Computers in biology and medicine*, 67:1–12.

Manna, P. R., Cohen-Tannoudji, J., Counis, R., Garner, C. W., Huhtaniemi, I., Kraemer, F. B., and Stocco, D. M. (2013). Mechanisms of action of hormone-sensitive lipase in mouse leydig cells its role in the regulation of the steroidogenic acute regulatory protein. *Journal of Biological Chemistry*, 288(12):8505–8518.

Manna, P. R., Dyson, M. T., and Stocco, D. M. (2009). Regulation of the steroidogenic acute regulatory protein gene expression: present and future perspectives. *Mol Hum Reprod*, 15(6):321–33.

Manna, P. R., Wang, X.-J., and Stocco, D. M. (2003). Involvement of multiple transcription factors in the regulation of steroidogenic acute regulatory protein gene expression. *Steroids*, 68(14):1125–1134.

McIlmoil, S., Call, G., Barney, M., Strickland, J., and Judd, A. (2015). Interleukin-6 inhibits adrenal androgen release from bovine adrenal zona reticularis cells by inhibiting the expression of steroidogenic proteins. *Domestic animal endocrinology*, 53:108–123.

McIlmoil, S., Strickland, J., and Judd, A. (2016). Interleukin 6 increases the in vitro expression of key proteins associated with steroidogenesis in the bovine adrenal zona fasciculata. *Domestic animal endocrinology*, 55:11–24.

Miller, W. L. (2013). Steroid hormone synthesis in mitochondria. *Molecular and cellular endocrinology*, 379(1):62–73.

Niakan, K. and McCabe, E. (2005). Dax1 origin, function, and novel role. *Molecular genetics and metabolism*, 86(1):70–83.

Nickerson, P. (1976). The adrenal cortex in spontaneously hypertensive rats. a quantitative ultrastructural study. *The American journal of pathology*, 84(3):545.

Osman, H., Murigande, C., Nadakal, A., and Capponi, A. M. (2002). Repression of dax-1 and induction of sf-1 expression two mechanisms contributing to the activation of aldosterone biosynthesis in adrenal glomerulosa cells. *Journal of Biological Chemistry*, 277(43):41259–41267.

Phillips, R., Kondev, J., and Theriot, J. (2009). Physical biology of the cell; garland science: New york, 2009.

Ragazzon, B., Lefrançois-Martinez, A.-M., Val, P., Sahut-Barnola, I., Tournaire, C., Chambon, C., Gachancard-Bouya, J.-L., Begue, R.-J., Veyssière, G., and Martinez, A. (2006). Adrenocorticotropin-dependent changes in sf-1/dax-1 ratio influence steroidogenic genes expression in a novel model of glucocorticoid-producing adrenocortical cell lines derived from targeted tumorigenesis. *Endocrinology*, 147(4):1805–1818.

Rankin, J., Walker, J. J., Windle, R., Lightman, S. L., and Terry, J. R. (2012). Characterizing dynamic interactions between ultradian glucocorticoid rhythmicity and acute stress using the phase response curve.

Reul, J. and Kloet, E. D. (1985). Two receptor systems for corticosterone in rat brain: microdistribution and differential occupation. *Endocrinology*, 117(6):2505–2511.

Sadasivam, M., Ramatchandirin, B., Balakrishnan, S., and Prahalathan, C. (2015). Tnf-α-mediated suppression of leydig cell steroidogenesis involves dax-1. *Inflammation Research*, 64(7):549–556.

Shen, W.-J., Patel, S., Natu, V., Hong, R., Wang, J., Azhar, S., and Kraemer, F. B. (2003). Interaction of hormone-sensitive lipase with steroidogeneic acute regulatory protein facilitation of cholesterol transfer in adrenal. *Journal of Biological Chemistry*, 278(44):43870–43876.

Song, K.-H., Park, Y.-Y., Park, K. C., Hong, C. Y., Park, J. H., Shong, M., Lee, K., and Choi, H.-S. (2004). The atypical orphan nuclear receptor dax-1 interacts with orphan nuclear receptor nur77 and represses its transactivation. *Molecular Endocrinology*, 18(8):1929–1940.

Spiga, F. and Lightman, S. L. (2015). Dynamics of adrenal glucocorticoid steroidogenesis in health and disease. *Molecular and cellular endocrinology*, 408:227–234.

Spiga, F., Liu, Y., Aguilera, G., and Lightman, S. L. (2011a). Temporal effect of adrenocorticotrophic hormone on adrenal glucocorticoid steroidogenesis: involvement of the transducer of regulated cyclic amp-response element-binding protein activity. *J Neuroendocrinol*, 23(2):136–42.

Spiga, F., Waite, E. J., Liu, Y., Kershaw, Y. M., Aguilera, G., and Lightman, S. L. (2011b). Acth-dependent ultradian rhythm of corticosterone secretion. *Endocrinology*, 152(4):1448–57.

Spiga, F., Walker, J. J., Gupta, R., Terry, J. R., and Lightman, S. L. (2015). 60 years of neuroendocrinology: Glucocorticoid dynamics: insights from mathematical, experimental and clinical studies. *Journal of Endocrinology*, 226(2):T55–T66.

Spiga, F., Walker, J. J., Terry, J. R., and Lightman, S. L. (2014). Hpa axis-rhythms. *Compr Physiol*, 4(3):1273–98.

Sugawara, T., Kiriakidou, M., McAllister, J. M., Holt, J. A., Arakane, F., and Strauss, J. F. (1997a). Regulation of expression of the steroidogenic acute regulatory protein (star) gene: a central role for steroidogenic factor 1. *Steroids*, 62(1):5–9.

Sugawara, T., Kiriakidou, M., McAllister, J. M., Kallen, C. B., and Strauss, J. F. (1997b). Multiple steroidogenic factor 1 binding elements in the human steroidogenic acute regulatory protein gene 5'-flanking region are required for maximal promoter activity and cyclic amp responsiveness. *Biochemistry*, 36(23):7249–7255.

Swinburne, I. A. and Silver, P. A. (2008). Intron delays and transcriptional timing during development. *Developmental cell*, 14(3):324–330.

Tkachenko, I. V., Jääskeläinen, T., Jääskeläinen, J., Palvimo, J. J., and Voutilainen, R. (2011). Interleukins 1α and 1β as regulators of steroidogenesis in human nci-h295r adrenocortical cells. *Steroids*, 76(10):1103–1115.

Veitia, R. A. (2002). Exploring the etiology of haploinsufficiency. *Bioessays*, 24(2):175–184.

Waite, E. J., McKenna, M., Kershaw, Y., Walker, J. J., Cho, K., Piggins, H. D., and Lightman, S. L. (2012). Ultradian corticosterone secretion is maintained in the absence of circadian cues. *European Journal of Neuroscience*, 36(8):3142–3150.

Walker, J. J., Terry, J. R., and Lightman, S. L. (2010). Origin of ultradian pulsatility in the hypothalamic-pituitary-adrenal axis. *Proc Biol Sci*, 277(1688):1627–33.

Watt, M. J., Holmes, A. G., Pinnamaneni, S. K., Garnham, A. P., Steinberg, G. R., Kemp, B. E., and Febbraio, M. A. (2006). Regulation of hsl serine phosphorylation in skeletal muscle and adipose tissue. *American Journal of Physiology-Endocrinology and Metabolism*, 290(3):E500–E508.

Windle, R., Wood, S., Shanks, N., Lightman, S., and Ingram, C. (1998). Ultradian rhythm of basal corticosterone release in the female rat: Dynamic interaction with the response to acute stress 1. *Endocrinology*, 139(2):443–450.

Winnay, J. N. and Hammer, G. D. (2006). Adrenocorticotropic hormone-mediated signaling cascades coordinate a cyclic pattern of steroidogenic factor 1-dependent transcriptional activation. *Mol Endocrinol*, 20(1):147–66.

Xu, B., Yang, W. H., Gerin, I., Hu, C. D., Hammer, G. D., and Koenig, R. J. (2009). Dax-1 and steroid receptor rna activator (sra) function as transcriptional coactivators for steroidogenic factor 1 in steroidogenesis. *Mol Cell Biol*, 29(7):1719–34.

Zhao, D., Duan, H., Kim, Y. C., and Jefcoate, C. R. (2005). Rodent star mrna is substantially regulated by control of mrna stability through sites in the 3'-untranslated region and through coupling to ongoing transcription. *J Steroid Biochem Mol Biol*, 96(2):155–73.

Æsøy, R., Mellgren, G., Morohashi, K.-I., and Lund, J. (2002). Activation of camp-dependent protein kinase increases the protein level of steroidogenic factor-1. *Endocrinology*, 143(1):295–303.